

Coalescence and linkage disequilibrium in facultatively sexual diploids

Matthew Hartfield^{1,*,\dagger}, Stephen I. Wright^{*}, and Aneil F. Agrawal^{*}

9th August 2018

* Department of Ecology and Evolutionary Biology, University of Toronto,
Ontario, Canada.

\dagger Bioinformatics Research Centre, Aarhus University, Aarhus C 8000, Denmark.

¹ *Corresponding author:* matthew.hartfield@birc.au.dk

Running Head: Linkage Disequilibrium under partial sex

Key words: Facultative sex, coalescent theory, crossing over, recombination,
gene conversion, linkage disequilibrium

Website for simulation code:

<http://github.com/MattHartfield/FacSexCoalescent>

Abstract

2 Under neutrality, linkage disequilibrium (LD) results from physically
linked sites having non-independent coalescent histories. In obligately sexual
4 organisms, meiotic recombination is the dominant force separating linked
variants from one another, and thus in determining the decay of LD with
6 physical distance. In facultatively sexual diploid organisms that principally
reproduce clonally, mechanisms of mitotic exchange are expected to become
8 relatively more important in shaping LD. Here we outline mathematical and
computational models of a facultative-sex coalescent process that includes
10 meiotic and mitotic recombination, via both crossovers and gene conversion,
to determine how LD is affected with facultative sex. We demonstrate that
12 the degree to which LD is broken down by meiotic recombination simply
scales with the probability of sex if it is sufficiently high (much greater than
14 $1/N$ for N the population size). However, with very rare sex (occurring with
frequency on the order of $1/N$), mitotic gene conversion plays a particularly
16 important and complicated role because it both breaks down associations
between sites and removes within-individual diversity. Strong population
18 structure under rare sex leads to lower average LD values than in panmictic
populations, due to the influence of low-frequency polymorphisms created
20 by allelic sequence divergence acting in individual subpopulations. These
analyses provide information on how to interpret observed LD patterns in
22 facultative sexuals, and determine what genomic forces are likely to shape
them.

24 Introduction

25 Coalescent theory is a powerful mathematical framework that is used to determine
26 how natural selection and demographic history affect genetic diversity (Kingman
1982; Rosenberg and Nordborg 2002; Hein *et al.* 2005; Wakeley 2009). Tradi-
28 tional coalescent models assume that the population is obligately sexual, but there
has been less attention on creating models that account for different reproductive
30 modes. While the coalescent with self-fertilisation has been extensively studied
(Nordborg and Donnelly 1997; Nordborg 1997, 2000; Nordborg and Krone 2002),
32 little theory exists on coalescent histories in organisms with other mixed repro-
ductive systems.

34 Previous theory has investigated genetic diversity in facultatively sexual dip-
loid organisms, which reproduce via a mixture of sexual and parthenogenetic re-
36 production (Brookfield 1992; Burt *et al.* 1996; Balloux *et al.* 2003; Bengtsson 2003;
Cepititis 2003). A general result arising from this work is that when an organism
38 exhibits very rare population-level rates of sex ($\sigma \leq \mathcal{O}(1/N)$, for σ the probability
of sex and N the population size), they will exhibit ‘allelic sequence divergence’
40 where both alleles within a diploid individual accumulate distinct polymorphisms
from each other (Mark Welch and Meselson 2000; Butlin 2002). Hartfield *et al.*
42 (2016) subsequently investigated a coalescent model of facultative sexuals, and
quantified how the presence of gene conversion can reduce within-individual di-
44 versity to less than that expected in sexual organisms, contrary to the effects of
allelic sequence divergence. Hence these results provide a potential explanation as
46 to why allelic divergence is not widely observed in empirical studies of facultatively
sexual organisms (reviewed in Hartfield (2016)).

48 However, this analysis only modelled the genetic history at a single, non-
recombining locus. Here, genealogies only greatly differed from those in obligately
50 sexual organisms at very low frequencies of sex ($\sigma \leq \mathcal{O}(1/N)$). As a consequence,
methods to estimate the frequency of sex can only do so based on the degree of
52 allelic sequence divergence, and are expected to be ineffective if the frequency of
sex is greater than $1/N$ and/or gene conversion is prevalent (Ceplitis 2003; Hart-
54 field *et al.* 2016). In contrast, many facultatively sexual organisms exhibit much
higher occurrences of sex. Pea aphids reproduce sexually about once every ten
56 to twenty generations (Jaquiéry *et al.* 2012), while *Daphnia* undergo one sexual
generation and five to twenty asexual generations a year (Haag *et al.* 2009). The
58 wild yeast *Saccharomyces paradoxus* has an outcrossing frequency of 0.001; while
low, this value is four orders of magnitude higher than $1/N_e$ (Tsai *et al.* 2008). If
60 we wish to create a general coalescent model that can be used to estimate rates
of sexual reproduction in species undergoing more frequent sex, then we need to
62 increase the power of this coalescent process to consider how patterns of genetic
diversity at multiple loci are affected with facultative sex.

64 This is achievable by considering how genealogies of multiple sites correlate
along a chromosome. Two completely linked sites will reach a common ancestor
66 in the past at the same time, so will share the same gene genealogy. However, if a
recombination event (e.g., via meiotic crossing over) were to separate the sites, each
68 sub-segment may have different genetic histories (Hudson 1983). Breaking apart
correlations between sites is reflected with lower linkage disequilibrium, which can
70 be measured from genomic data (Griffiths 1981; Hudson and Kaplan 1985; Hudson
1990; Simonsen and Churchill 1997; McVean 2002). Gene conversion can also break
72 apart correlations between sites through transferring genetic material across DNA

strands (Wiuf and Hein 2000).

74 As meiotic crossing over occurs during sexual reproduction, one may expect
that the extent to which linkage disequilibrium is broken down should scale with
76 the probability of sex (see Nordborg (2000) for a related argument for the co-
alescent with self-fertilisation). Tsai *et al.* (2008) used this logic to calculate the
78 frequency of sex in the yeast *Saccharomyces paradoxus*, by comparing effective pop-
ulation sizes inferred from linkage disequilibrium decay (which should scale with
80 the meiotic recombination rate, and therefore the rate of sex) with those from nuc-
leotide variation (which should be independent of sex if sufficiently high). Lynch
82 *et al.* (2017) used similar arguments to conclude that even though the facultatively
sexual water flea *Daphnia pulex* has a lower overall crossover recombination rate
84 than *Drosophila melanogaster*, it has a higher crossover rate when sex does occur.

However, the logic used in these studies assumes that the frequency of sex
86 only affects occurrences of meiotic crossing over. Low rates of sex also distort the
underlying genealogies, leading to subsequent events (including allelic sequence
88 divergence or removal of diversity via gene conversion) that also affect how poly-
morphisms are correlated along haplotypes. Hence these approaches may become
90 problematic in species exhibiting low rates of sexual reproduction, or if gene con-
version is an important force in shaping genetic diversity, as observed in empirical
92 studies of facultative sexuals (Crease and Lynch 1991; Schön *et al.* 1998; Normark
1999; Schön and Martens 2003; Flot *et al.* 2013).

94 We describe both mathematical theory and a routine for simulating multi-site
genealogies with facultative sex, allowing for both meiotic and mitotic crossover
96 recombination and gene conversion. We use these new models to investigate how
linkage disequilibrium patterns are affected in facultatively sexual organisms, and

98 how these results can be used to infer rates of sex from genome data. Specifically,
we investigate when the breakdown of linkage disequilibrium scales with sex, as
100 predicted by intuition, and when this logic does not hold.

102 **Overview of the facultative-sex coalescent and re- combination events**

Our primary goal is to examine how different frequencies of sex affects linkage
104 disequilibrium. Heuristically speaking, the expected strength of disequilibrium
depends on the probability that two sampled haplotypes (hereafter ‘samples’) co-
106 alesce before either haplotype is disrupted by recombination. Before presenting
the formal model, we begin by discussing how facultative sex affects coalescence
108 and then recombination.

In the standard coalescent, each member of a set of (non-recombining) samples
110 can be thought of as travelling independently backward in time through the gen-
erations. A coalescence event occurs if two samples independently “choose” the
112 same parental allele as their ancestor. The waiting time until the next coalescence
depends only the number of remaining samples but, importantly, not on “where”
114 the samples are currently found (i.e., in which individual organisms). However, for
diploids with a low frequency of sex, the “where” information is crucial (Bengtss-
116 son 2003; Ceplitis 2003; Hartfield *et al.* 2016). For example, two samples can be
the two haplotypes found in a single diploid individual (which we denote as ‘a
118 paired sample’) or they can each come from different individuals (which we denote
as ‘two unpaired samples’). The two haplotypes within a paired sample do not

120 travel back in time independently, rather they travel together for as long as repro-
duction is asexual. Coalescence between them is not possible for all the asexual
122 generations they remain paired (ignoring gene conversion). A sexual event splits
a paired sample into two unpaired samples that can then coalesce in a subsequent
124 generation. For this reason, paired samples are expected to have longer average
coalescence times than unpaired samples and low sex increases average coalescence
126 time compared to high sex (Bengtsson 2003; Ceplitis 2003; Balloux *et al.* 2003).
However, if the frequency of mitotic gene conversion is high relative to the fre-
128 quency of sex, then these predictions are reversed (Hartfield *et al.* 2016). In this
case, paired samples can coalesce faster than unpaired samples because each gen-
130 eration the samples are paired provides an opportunity for coalescence via mitotic
gene conversion.

132 In sum, low sex in diploids requires a ‘structured’ coalescent approach because
paired and unpaired samples behave differently; this structure affects the distri-
134 bution of coalescence times (including the mean and variance) and is sensitive to
the amount of mitotic gene conversion. Technically, this structure occurs even in
136 diploids that are obligately sexual; however, the coalescent can be safely modelled
ignoring the structure because the time spent in “paired” states is infinitesimally
138 brief on the coalescent timescale when sex is common. To affect coalescence times,
sex must be sufficiently uncommon, i.e. $\sigma \leq \mathcal{O}(1/N)$, where N is the population
140 size and σ is the fraction of offspring sexually produced each generation via the
random union of gametes (i.e., $\sigma = 1$ represents obligate sex and $\sigma = 0$ obligate
142 asexuality; see Table 1 for a list of symbol definitions).

Different sites along a genetic segment can have different genealogical histories
144 as long as there is some recombination. Low sex affects recombination in several

Symbol	Usage
N	Diploid population size (with $2N$ haplotypes), denoted N_T if measured across a subdivided population
f_A, f_B	Frequency of derived allele at site A, B
f_{AB}	Frequency of haplotypes carrying derived allele at both sites
D_{AB}	Disequilibrium between two sites, $f_{AB} - f_A f_B$
r^2	Standardised linkage disequilibrium, $D_{AB}/(f_A(1-f_A)f_B(1-f_B))$
r_d^2	'Ratio of means' measure of linkage disequilibrium, $E[D_{AB}]/(E[f_A(1-f_A)f_B(1-f_B)])$
$t_A(ij)$	Coalescent time at site A (if sampled from haplotypes i, j)
σ	Fraction of offspring produced via sex
c, c_A	Probability of meiotic (mitotic) crossing over between two sites
\tilde{c}, \tilde{c}_A	Probability of meiotic (mitotic) crossing over between two adjacent sites
γ_1, γ_2	Probability of mitotic gene conversion covering one, two sites (analytical model)
γ_{1S}, γ_{2S}	Probability of meiotic gene conversion covering one, two sites (analytical model)
g, g_S	Probability of mitotic (meiotic) gene conversion initiating at a site
Ω	Population-level frequency of sex, $2N\sigma$
ρ, ρ_A	Population-level rate of meiotic (mitotic) crossing over, $4Nc$ ($4Nc_A$)
$\tilde{\rho}_A$	Population-level rate of mitotic crossing over between two adjacent sites, $4N\tilde{c}_A$
Γ_1, Γ_{1S}	Population-level rate of mitotic (meiotic) gene conversion affecting a single site, $4N\gamma_1$ ($4N\gamma_{1S}$)
G	Population-level rate of gene conversion initiation, $4Ng$
λ, λ_S	Average length of mitotic (meiotic) gene conversion event
L	Number of sampled sites; $L - 1$ is number of breakpoints
Q, Q_S	Number of breakpoints in units of average gene conversion length (e.g. $Q = (L - 1)/\lambda$ for mitotic gene conversion)
R	Population-level meiotic crossing rate (simulation), $4N\tilde{c}(L - 1)$
Γ	Population-level mitotic gene conversion rate (simulation), $4Ng(L - 1)$
ϕ	Ratio of sex to mitotic gene conversion acting at a single site, $(\Omega Q)/\Gamma$
μ	Mutation rate over L sites
θ	Population level mutation rate, $4N\mu$
m	Probability of migration (island model)
M	Population-level rate of migration, $2N_T m$
p_1, p_2	Probability of one, two gene conversion breakpoints within sample

Table 1: Glossary of Notation.

ways. We consider both crossing-over (the reciprocal exchange of genetic material
146 between two haplotypes) and gene conversion (where genetic material is copied
from one haplotype to its homolog). When sexual reproduction is rare, the fre-
148 quency of meiotic recombination will necessarily be low. Mitotic crossovers and
mitotic gene conversion can then become important for two reasons. First, in
150 comparison to meiotic recombination, mitotic recombination becomes a relatively
more important route of genetic exchange as meiosis becomes rare. Second, in
152 paired samples (which are only an important consideration when sex is low), mi-
totic recombination can either lead to gene exchange (the splitting of a multisite
154 sample into separate pieces) or coalescence.

Figure 1 outlines the possible outcomes for recombination under facultative
156 sex. Going back in time, sex involving a meiotic crossover will transform an un-
paired sample into a paired sample (i.e., the unpaired sample descended from the
158 two homologs in the parent; Figure 1(a)). For a paired sample, sex segregates the
two samples into separate parents, creating two unpaired samples (Figure 1(b)).
160 However, if a crossover also occurred on one of these samples, then the affected
sample becomes a paired sample in the parent; the overall outcome is a new paired
162 sample in one parent (each containing a section of ancestral material), and one un-
paired sample in the other parent (Figure 1(c)). Mitotic crossovers can also act in
164 paired samples unaffected by sex, swapping genetic material between homologues
(Figure 1(d)).

166 Gene conversion can affect a sample in several ways, where (i) gene conver-
sion initiates outside a tract of ancestral material but finishes within it; (ii) gene
168 conversion begins within a tract of ancestral material but extends beyond it; (iii)
both conversion breakpoints lie within ancestral material; or (iv) gene conversion

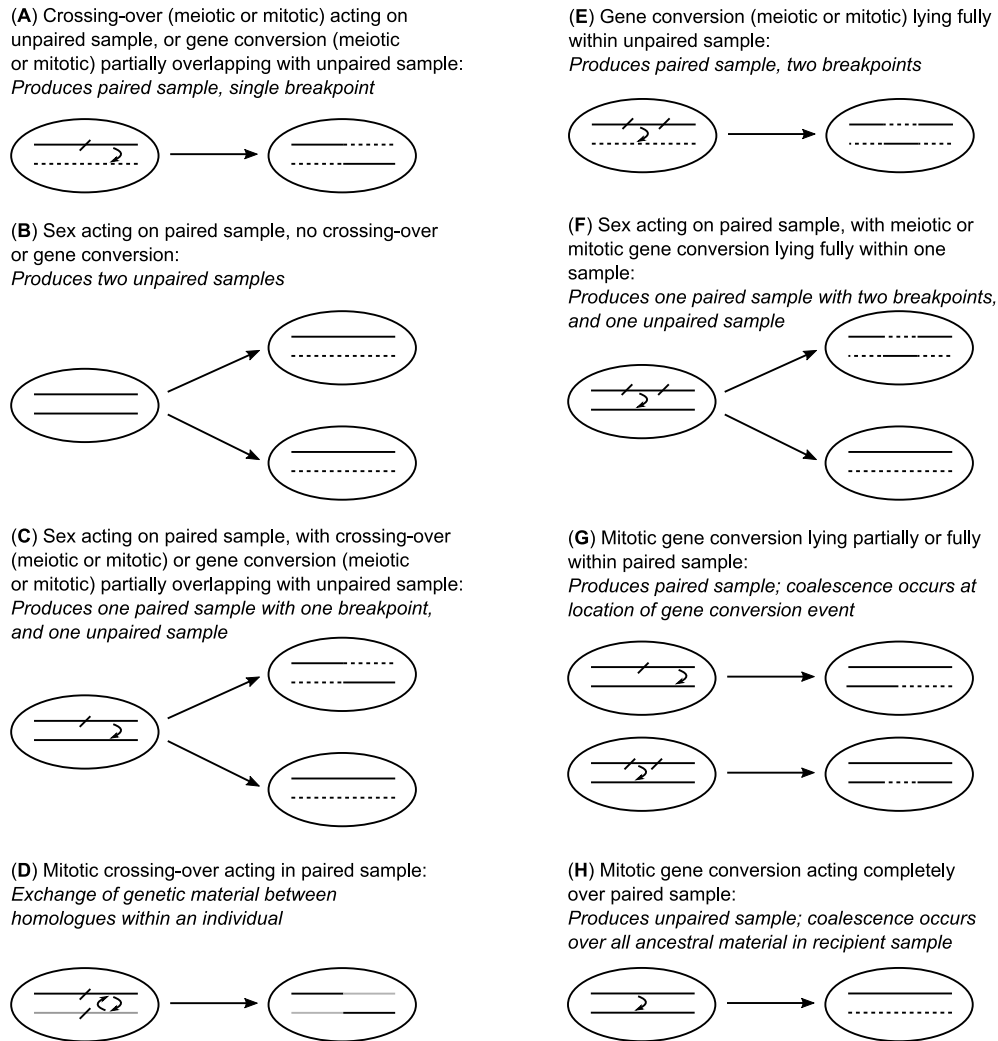


Figure 1: Schematic of different outcomes following gene exchange in the facultative-sex coalescent. Solid lines represent ancestral material; dotted lines represent non-ancestral material. Outcomes are described for (a) meiotic crossing over acting on an unpaired sample, or gene conversion acting on an unpaired sample that only partially overlaps with the haplotype; (b) sex acting on a paired sample with no crossing over or gene conversion; (c) both sex and either crossing over, or gene conversion that only partially overlaps with the haplotype, acting on a paired sample; (d) mitotic crossing over acting on a paired sample; (e) gene conversion (meiotic or mitotic) acting on an unpaired sample, which fully lies within the sampled haplotype; (f) both sex and gene conversion (lying fully within a haplotype) acting on a paired sample; (g) mitotic gene conversion acting on a segment of a paired sample; (h) mitotic gene conversion acting over the entire length of a paired sample (or over all remaining extant material).

170 acts over all ancestral material in a paired sample (see Wiuf and Hein (2000) for a
detailed discussion of the coalescent with gene conversion applicable to obligately
172 sexual diploids). If gene conversion acts on an unpaired sample, then it becomes
a paired sample with each haplotype carrying a segment of ancestral material,
174 which is a similar outcome to that following a crossover (Figure 1(e)). There are
either one or two breakpoints, depending on whether gene conversion lies partly or
176 fully within ancestral material. If acting on paired samples, the outcome depends
on whether sex has segregated the samples into different individuals. If so then
178 one of the two parents contains a paired sample with each part carrying ances-
tral material (Figure 1(f)). If not, then a segment of one sample coalesces into
180 the other (Figure 1(g)). Finally, mitotic gene conversion acting completely over
a paired sample reproducing asexually causes complete coalescence of one paired
182 sample, converting it into an unpaired sample. This outcome is equivalent to ‘gene
conversion’ for the single-site coalescent model (Hartfield *et al.* 2016) (Figure 1(h)).

184 Overall, facultative sex will affect linkage disequilibrium for at least three reasons.
First, the population-level rate of meiotic recombination will be proportional
186 to the frequency of sexual reproduction. Second, when sex becomes very rare, the
rate and patterns of coalescence change substantially, which is important because
188 disequilibrium is affected by the rate of recombination relative to coalescence.
Third, in the low-sex regime, mitotic gene conversion can become important as it
190 becomes a key coalescence mechanism for a paired sample; alternatively, a single
haplotype within an individual can be separated (with either one or two break-
192 points) via gene conversion.

Two-site analytical model

194 A commonly used metric of linkage disequilibrium is (Hill and Robertson 1968):

$$r^2 = \frac{D_{AB}^2}{f_A(1-f_A)f_B(1-f_B)} \quad (1)$$

where f_i is the frequency of the derived allele at site i ($i = A$ or B), and $D_{AB} =$
196 $f_{AB} - f_A f_B$ with f_{AB} being the frequency of haplotypes carrying the derived allele
at both sites. A related quantity

$$r_d^2 = \frac{E[D_{AB}^2]}{E[f_A(1-f_A)f_B(1-f_B)]} \quad (2)$$

198 has been studied in analytical neutral models (Ohta and Kimura 1971; Weir and
Hill 1986; McVean 2002) (we use r_d^2 to represent this quantity, rather than the
200 traditional symbol σ_d^2 , to avoid confusion with σ that is used to parameterize the
frequency of sex in this analysis). r_d^2 overestimates the expected value of r^2 but
202 the discrepancy is reduced if it is only applied to sites where the minor allele is not
too rare (McVean 2002). In the classic analyses, which is applicable to obligately
204 sexual diploids:

$$r_d^2 \approx \frac{10 + 2\rho}{22 + 26\rho + 4\rho^2} \quad (3)$$

where $\rho = 4Nc$ with c being the per-generation probability of meiotic crossing
206 over between two sites. McVean (2002) showed that a coalescence approach can
be used to derive this result, demonstrating that r_d^2 is a function of the covariance
208 in coalescence times between two sites. The goal here is to quantify how r_d^2 is
altered by facultative sex. We use the coalescent approach of McVean (2002) for

210 a two-site model in a diploid population of size N . Two samples at each of two
sites in a diploid model can occur in 17 different states, as outlined in Figure 2.
212 In the traditional haploid model, only 7 states are necessary, but here we must
consider the full 17-state model to consider the pairing of haplotypes. The model
214 is presented in detail in Section A of Supplementary Mathematica File S1, with
an overview provided in Figure 2.

216 The first key step in constructing the model is to derive the transition matrix
giving the probabilities (going backwards in time) of changing states. These prob-
218 abilities depend on the biology of reproduction and inheritance. If meiosis occurs,
there is a crossover between sites A and B with probability c . The probability of
220 a mitotic crossover is c_A per generation (which does not require meiosis). Regard-
less of reproductive mode, mitotic gene conversion can occur. With probability γ_2
222 there is a mitotic gene conversion event whose tract length covers both sites. With
probability γ_1 a mitotic gene conversion event occurs where one end of the gene
224 conversion tract lies at the breakpoint between the two sites, and the other end
lies beyond them (γ_{1S} is the analogous probability for a meiotic gene conversion
226 event, conditional on meiosis occurring). It is worth noting that γ_1 enters the
transition matrix for two separate reasons. It determines the probability that one
228 site coalesces via mitotic gene conversion (e.g., transition from state S2 to S14;
see Figure 2) and it determines the probability that samples at different sites on
230 the same haplotype get split onto separate haplotypes by mitotic gene conversion
(e.g., transition from state S3 to S9; see Figure 2). Note that gene conversion
232 involving one site is functionally equivalent to a crossing-over event. Using these
parameters, the construction of the transition matrix is tedious but straightfor-
234 ward. In contrast, γ_2 only enters transitions involving coalescence affecting one

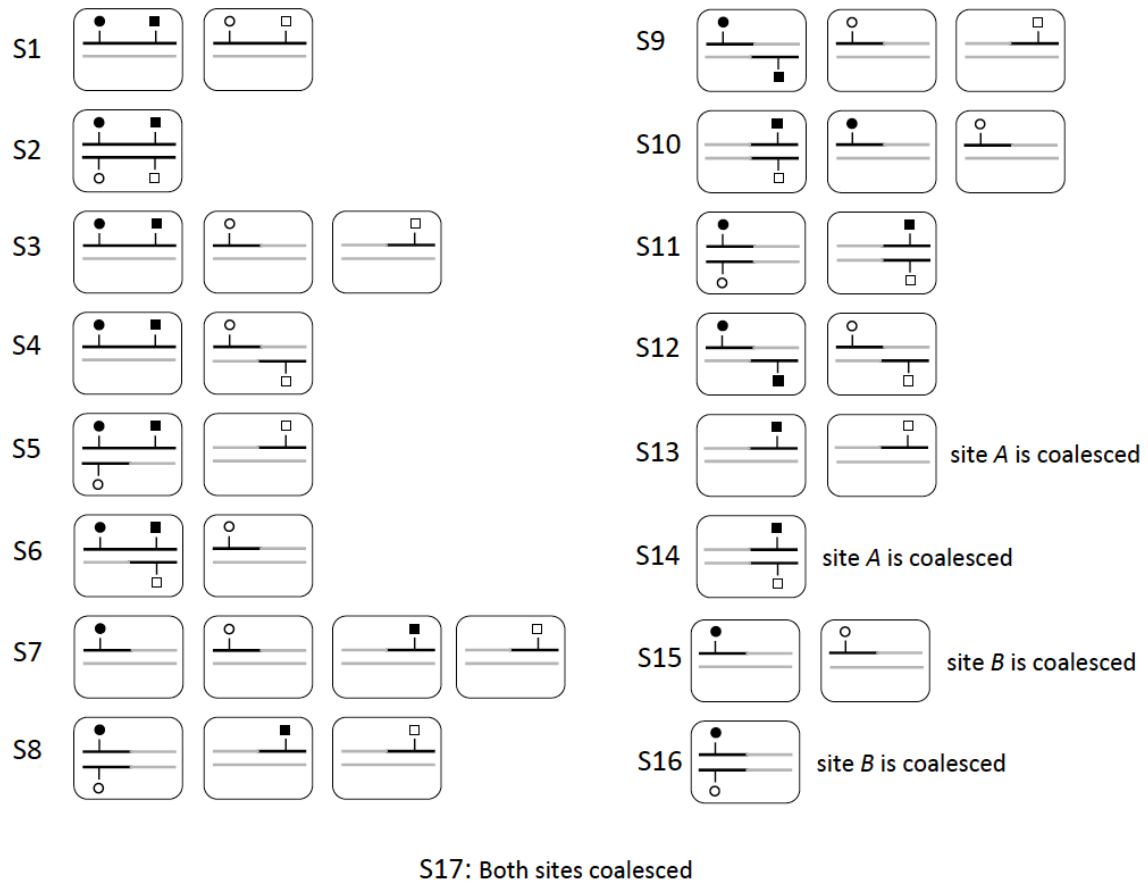


Figure 2: The 17 possible states for two copies of each of two sites, for the analytical model. Each rounded rectangle represents a separate diploid individual. The two focal copies of the *A* site are represented by open and closed circles. The two focal copies of the *B* site are represented by open and closed squares. The shading of symbols, i.e., open vs. closed, has no meaning other than to distinguish focal copies. Haplotypes or parts of haplotypes that do not carry ancestral material (i.e., not carrying focal copies) are shown in grey. Coalesced sites are not shown.

or both sites. Using first-step analysis (Wakeley 2009, Chapter 7) and following
236 McVean (2002), we construct a system of equations for the expected value of the
product of coalescent times at the two sites, given their current state z . These
238 equations capture the expected time for the system to move out of the state z ,
before calculating the expected coalescent time of either one or both sites, given
240 the new state k . These equations have the form:

$$\begin{aligned} E[t_A t_B | Z = z] &= E[\tau_z^2] + E[\tau_z] \sum_{k \neq z} P_{zk} E[t_A | Z = k] \\ &\quad + E[\tau_z] \sum_{k \neq z} P_{zk} E[t_B | Z = k] \\ &\quad + \sum_{k \neq z} P_{zk} E[t_A t_B | Z = k] \end{aligned} \quad (4)$$

where τ_z is the time to exit state z , P_{zk} is the probability that the system moves
242 from state z to state k conditional on leaving state z , and $E[t_x | Z = k]$ is the
expected time to coalescence of site x given it is currently in state k . As described
244 in Section A of Supplementary Mathematica File S1, these components can be
calculated from the transition matrix, either directly for discrete time or after
246 appropriate transformation for the continuous time approximation (Möhle 1998;
Wakeley 2009).

248 Following McVean (2002):

$$r_d^2 = \frac{E[t_{A(ij)} t_{B(ij)}] - 2E[t_{A(ij)} t_{B(ik)}] + E[t_{A(ij)} t_{B(kl)}]}{E[t_{A(ij)} t_{B(kl)}]} \quad (5)$$

where $E[t_{A(ij)} t_{B(kl)}]$ is the expected product of the coalescent times at site A ,
250 where the two copies are sampled from haplotypes i and j , and at site B , where

the two copies are sampled from haplotypes k and l (and different indexes denote
 252 other haplotype samples). Analogous to measuring r_d^2 from haploids where each
 haplotype represents an independent sample, we calculate r_d^2 assuming that each
 254 haplotype comes from a different individual (Figure 2) so that the three terms in
 the numerator represent coalescence times from states S1, S3, and S7.

256 We first consider the case of partial asexuality where sex may be rare at the
 individual level but is not too rare at the population level (i.e., $0 < \sigma \leq 1$ but
 258 $N\sigma \gg 1$). We find

$$r_d^2 = \frac{10 + \Psi}{(2 + \Psi)(11 + \Psi)} \quad (6)$$

where $\Psi = \rho\sigma + \rho_A + (1/2)\Gamma_1 + (1/2)\sigma\Gamma_{1S}$ with scaled parameters $\rho = 4Nc$,
 260 $\rho_A = 4Nc_A$, $\Gamma_1 = 4N\gamma_1$, and $\Gamma_{1S} = 4N\gamma_{1S}$. Simplifying the model by ignoring
 gene conversion and mitotic crossing over ($\Gamma_1 = \Gamma_{1S} = \rho_A = 0$), the result above
 262 is the same as the obligate sex result (Equation 3) but using an effective scaled
 crossover rate $\rho\sigma$ in place of ρ (Figure 3(a)).

264 We next consider the case where sex is rare at the population level, $2N\sigma \rightarrow \Omega$
 as $N \rightarrow \infty$. In the absence of mitotic gene conversion or mitotic crossing over
 266 ($\Gamma_1 = \rho_A = 0$) then:

$$r_d^2 = \frac{1728 + 3960\Omega + 3870\Omega^2 + 2091\Omega^3 + 634\Omega^4 + 95\Omega^5 + 5\Omega^6}{1728 + 4824\Omega + 5958\Omega^2 + 3927\Omega^3 + 1342\Omega^4 + 209\Omega^5 + 11\Omega^6} + \mathcal{O}(\xi) \quad (7)$$

where the rates of disruptive meiotic processes c , $\gamma_{1S} \sim \mathcal{O}(\xi)$ with ξ being a small
 268 term ($|\xi| \ll 1$). Equations 6 and 7 differ in several important ways. First their
 maximum values, and the conditions to achieve these maxima, differ. The max-

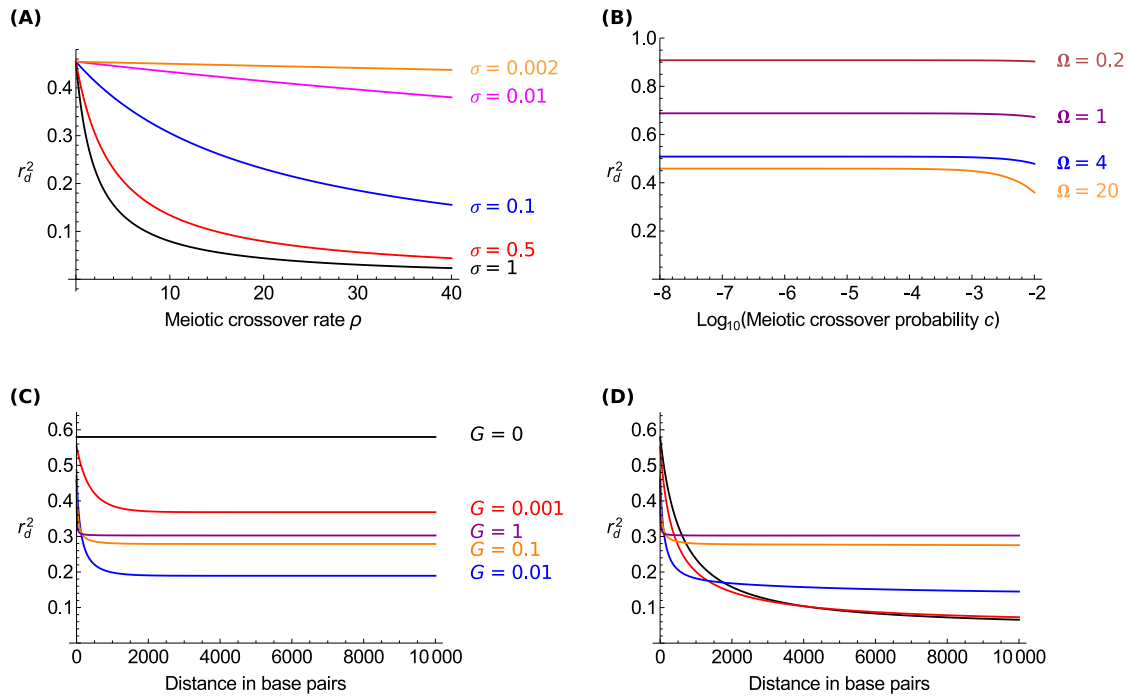


Figure 3: (a) Linkage disequilibrium, measured as r_d^2 , when sex is high at the population level (i.e., $\sigma \gg \mathcal{O}(1/N)$), measured as a function of the meiotic crossover rate ρ . Different frequencies of sex (σ) are shown. Other parameters: $c_A = \gamma_1 = \gamma_2 = \gamma_{1S} = 0$. (b) r_d^2 when the frequency of sex is low ($\sigma \sim \mathcal{O}(1/N)$) and the only haplotype disrupting force is meiotic crossing over ($c > 0$). Different rates of sex ($\Omega = 2N\sigma$) are shown. Other parameters: $c_A = \gamma_1 = \gamma_2 = \gamma_{1S} = 0$. (c, d) r_d^2 when the frequency of sex is low ($\sigma \sim \mathcal{O}(1/N)$) as a function of the distance between two sites (measured in basepair distance), for different levels of mitotic gene conversion ($G = 4Ng$). Results are shown without (c) and with (d) mitotic crossing-over (i.e., $\tilde{\rho}_A = 4N\tilde{c}_A$ with $\tilde{\rho}_A = 0$ in (c) and $\tilde{\rho}_A = 0.002$ in (d)). Other parameters: $\lambda = 500$; $\Omega = 2$ (see Figure A in Supplementary File S2 for similar plots using different Ω values).

imum value of Equation 6 occurs as the haplotype disrupting forces (crossovers and gene conversion) become small, i.e., $r_d^2 \rightarrow 10/22 \approx 0.45$ as $\Psi \rightarrow 0$. In contrast, the maximum value of Equation 7 occurs as sex becomes increasingly rare, i.e., $r_d^2 \rightarrow 1$ as $\Omega \rightarrow 0$. Second, r_d^2 in Equation 6 has a strong dependence on physical distance because disruption via crossover or gene conversion is an increasing function of distance, i.e., Ψ is implicitly an increasing function of distance. In contrast Equation 7 is very weakly dependent on physical distance through terms of $\mathcal{O}(\xi)$ (Figure 3(b)).

Equation 7 assumes no mitotic gene conversion or mitotic crossing over but important changes to r_d^2 occur with either of these processes. An analytical approximation can be obtained but the expression is unwieldy (Section A of Supplementary Mathematica File S1). Both types of mitotic gene conversion events, represented via $\Gamma_1 = 4N\gamma_1$ and $\Gamma_2 = 4N\gamma_2$, as well as mitotic crossing over ($\rho_A = 4Nc_A$) affect the leading-order term for r_d^2 and are functions of the distance between sites. Mitotic crossing over can be modelled as a linear function of distance d , $c_A(d) = \tilde{c}_A d$. Using a standard assumption of exponentially distributed gene conversion tract lengths (Wiuf and Hein 2000), the probabilities of mitotic gene conversion are given by $\gamma_1(d) = 2g\lambda(1 - \exp(-d/\lambda))$ and $\gamma_2(d) = g\lambda \exp(-d/\lambda)$ where λ is the average tract length and g is the probability of gene conversion initiation per base pair (more precisely, per breakpoint between adjacent base pairs). The derivation is provided in Section A of Supplementary Mathematica File S1.

Figure 3(c) shows that r_d^2 declines with physical distance when there is mitotic gene conversion but no mitotic crossing over. Note that r_d^2 does not decline down to 0 with distance as it does in the classic model (Equation 3) of meiotic crossing over. Because gene conversion probabilities change slowly for $d/\lambda > 2$, there is

little decline in r_d^2 beyond this point. Surprisingly, r_d^2 is not always a monotonically
296 declining function of the probability of gene conversion initiation, g (or the scaled
parameter $G = 4Ng$), especially when $d > \lambda$ (Figure B(a) in Supplementary File
298 S2). Consequently, a species with a lower frequency of gene conversion events (i.e.,
smaller g) can have larger r_d^2 for small d but smaller r_d^2 for large d compared to
300 an otherwise similar species with larger g (Figure 3(c)). This behaviour of r_d^2 with
respect to g is likely due to the dual (and conflicting) roles of gene conversion in
302 increasing both the probability of coalescence and disruption of haplotypes. In
contrast, mitotic crossing over, which only affects haplotype disruption, affects r_d^2
304 monotonically as expected (Figure B(b) in Supplementary File S2). The addition
of mitotic crossing over reduces the minimum value of r_d^2 (Figure 3(d)). Even
306 with mitotic crossing over, r_d^2 does not go to zero at large distances and can
be considerably greater than zero when gene conversion is high (see Section A
308 of Supplementary Mathematica File S1). The minimum value reached by r_d^2 is
independent of the rate of mitotic crossing over (provided it is not zero) though
310 the distance at which the minimum is reached is shorter with higher rates of mitotic
crossing over.

312 **Simulation Algorithm**

We have previously developed an algorithm to build genealogies of facultative
314 sexual organisms at a single non-recombining locus (Hartfield *et al.* 2016). This
algorithm simulates genealogies of n samples, of which $2x$ are paired and the re-
316 maining $y = n - 2x$ samples are unpaired. The algorithm proceeds in a similar
manner as other coalescent simulations, in that it tracks the genetic histories of

318 samples into the past, sequentially enacting events that affect the genetic history
(e.g. coalescence, sexual reproduction). The relative probability of each event oc-
320 ccurring per generation is used to determine what the next event is, and at which
time in the past it arises. To further investigate the effects of facultative sex on
322 linkage disequilibrium, we extended this previous routine to consider coalescent
histories of multiple sites, and how various recombination phenomena affect how
324 genetic histories are correlated along chromosomes. In Appendix A we describe
how the crossover routine of Hudson (1983) and the gene conversion routine of
326 Wiuf and Hein (2000) are extended to consider the effects of facultative sex. As a
consequence, the updated coalescent simulation now models the effects of meiotic
328 and mitotic recombination on facultative sex, the outcomes of which are summar-
ised in Figure 1.

330 **Measuring linkage disequilibrium from simulations**

We used the updated coalescent simulation to calculate expected linkage disequilib-
332 rium in facultatively sexual organisms. Following a single simulation of a coalescent
process, a series of j genealogies are produced, one for each non-recombined part
334 of the genetic segment. Polymorphisms are added to each branch of the genealogy,
drawn from a Poisson distribution with mean $(1/2)\theta_j\tau_{i,j}$, for $\theta_j = 4N_T\mu(l_j/L)$ the
336 mutation rate of the segment covering l_j of L total sites given μ is the mutation
rate for a segment of L sites, and $\tau_{i,j}$ the length of branch i in segment j .

338 For each simulation, we measured linkage disequilibrium $D = f_{AB} - f_A f_B$ over
each pairwise combination of polymorphisms; this measure was then normalised
340 to $r^2 = D^2 / (f_A f_B (1 - f_A)(1 - f_B))$. Once r^2 was measured over all simulations,

values were placed into 20 equally-sized bins based on the distance between the two
342 polymorphisms. However, the number of pairwise samples were different for each
of the 20 bins. Samples in the last two bins produced noisy estimates of linkage
344 disequilibrium, so we only reported linkage disequilibrium estimates from the first
18 bins. We randomly subsampled data in bins 1 to 18 so that they include the
346 same number of pairwise comparisons as in the smallest bin that contained data,
to standardise bin size per simulation. Mean values per bin were recorded for
348 each simulation run. We then calculated the mean of means per bin over all 1,000
simulations, omitting points where data was not present in a bin for a simulation.
350 95% confidence intervals were calculated as $\pm \tilde{t}(s/\sqrt{n})$ for s the standard deviation
for the bin, n the number of points in the bin (maximum of 1,000, one for each
352 simulation run), and \tilde{t} the 97.5% quantile for a t -distribution with $n - 1$ degrees
of freedom.

354 **Measuring correlation in coalescence time between sites**

For some cases with low sex and mitotic gene conversion, we measured the correla-
356 tion in coalescence times between sites as a function of the distance between them,
to investigate how these values relate to observed linkage disequilibrium patterns.
358 For each simulation run, we obtained the number of non-recombined regions, and
the times at which the ancestral segment of that region for each individual co-
360 alesced. If more than 100 segments existed, these were subsampled down to 100.
We calculated the Pearson correlation in coalescent times for all segments; values
362 were then placed into one of 20 bins based on the distance between blocks (the
location of each segment was given by its midpoint). Values were only reported

364 for the first 18 bins, with further subsampling performed on bins 1 to 18 so they
contained the same number of comparisons as the smallest bin that contained data
366 for that simulation. The mean bin value for a simulation, as well as the mean of
means over all simulations and 95% confidence intervals were calculated using the
368 same method as for linkage disequilibrium measurements.

Data Availability

370 This new simulation program, *FacSexCoalescent*, along with documentation is
available from <http://github.com/MattHartfield/FacSexCoalescent>. We
372 first rebuilt the single-locus simulation program in C to greatly increase execu-
tion speed, before adding the crossover and gene conversion routines. As with the
374 previous version of the simulation, *FacSexCoalescent* uses a timescale of $2N$ gen-
erations while *ms* uses $4N$ generations. The documentation specifies other cases
376 where *FacSexCoalescent* inputs and outputs differ from other coalescent simula-
tions. We performed various tests of the simulation as described in Section B of
378 Supplementary File S2.

Supplementary File S1 is a *Mathematica* notebook of analytical derivations.
380 Supplementary File S2 contains additional results and figures. Supplementary
File S3 is a copy of the simulation code and manual. Supplemental files have also
382 been uploaded to FigShare.

Simulation Results

384 Linkage disequilibrium with crossing over

High frequencies of sex

386 We looked at how patterns of linkage disequilibrium are affected by crossovers, when sexual reproduction is frequent (that is, the scaled rate of sex $N\sigma \gg 1$).
388 Analytical results (Equation 6) suggest that the effect of meiotic crossovers on linkage disequilibrium is equal to that observed in an obligately sexual population
390 with a rescaled probability $c_{eff} = c\sigma$ (for $c = \tilde{c}d$ the crossover probability over distance d). To further investigate this pattern, we simulated genealogies over
392 $L = 1,001$ sites with a fixed population-level meiotic crossover rate over the entire ancestral segment $R = 4N\tilde{c}(L - 1) = 40$, which acts during sexual reproduction.
394 Results are reported over the first 900 sites.

Figure 4(a) plots how linkage disequilibrium decays over this region with differ-
396 ent probabilities of sex, varying from $\sigma = 1$ (i.e., obligate sex) to $\sigma = 0.002$. As expected, the decay in linkage disequilibrium is weakened with lower sex, since there
398 exists fewer opportunities for crossovers to act (compare Figure 4(a) to analytical expectations in Figure 3(a)). We confirm that the observed decay is equivalent
400 to an obligately sexual population with $c_{eff} = c\sigma$ in three ways. First, we ran equivalent (but haploid and sexual) simulations in `ms` using the rescaled crossover
402 probability, and observed that the decay in linkage disequilibrium matches results from the facultative-sex simulation (Figure 4(b)). Second, we used the ‘pairwise’
404 routine in the `LDhat` software (McVean *et al.* 2002) to estimate crossover rates from facultative-sex simulation data, and observed that they scaled linearly with

406 σ (Figure 4(c)). Finally, Figure 4(d) plots linkage disequilibrium values for all
facultative-sex coalescent simulations as a function of the effective recombination
408 rate, alongside the analytical expectation for r_d^2 (Equation 6). r^2 is calculated
after removing sites with minor allele frequency $< 10\%$, as r_d^2 is known to overes-
410 timate r^2 if all allele frequencies are considered. We see that the decay in linkage
disequilibrium over all simulations is close to, but slightly overshoots the theoret-
412 ical expectation (Equation 6). Similar behaviour was observed by McVean (2002,
Figure 3; compare solid line to square points).

414 **Low frequencies of sex**

When the probability of sex is low (i.e., $N\sigma \leq \mathcal{O}(1)$), samples will diverge within
416 individuals (Balloux *et al.* 2003; Bengtsson 2003; Ceplitis 2003; Hartfield *et al.*
2016). We examined how this allelic sequence divergence affects linkage disequilib-
418 rium by running simulations with $N\sigma \sim \mathcal{O}(1)$ (specifically we investigated $2N\sigma =$
 $\Omega = 20, 2$ and 0.2), but with a fixed scaled crossover rate $4N\tilde{c}(L-1)\sigma = R\sigma = 0.1$.
420 Although this scaled crossover rate is low, there is a high crossover rate when sex
does occur, hence we expect to see some breakdown of linkage disequilibrium
422 along the simulated genotype. We ran simulations over a larger number of sites
($L = 100,001$) so there was enough distance to observe a decay in disequilibrium.

424 Figure 5(a) displays the linkage disequilibrium observed in low-sex cases, along
with analytical expectations (Equation 7). After removing sites with minor allele
426 frequency less than 10% , the $\Omega = 20$ simulation exhibits r^2 close to 0.45 , which
is as given by Equation 6 as the crossover rate goes to zero. However, lower
428 rates of sex result in higher values of linkage disequilibrium, indicating that classic
estimates of r^2 using the rescaled recombination rate $R\sigma$ do not properly quantify

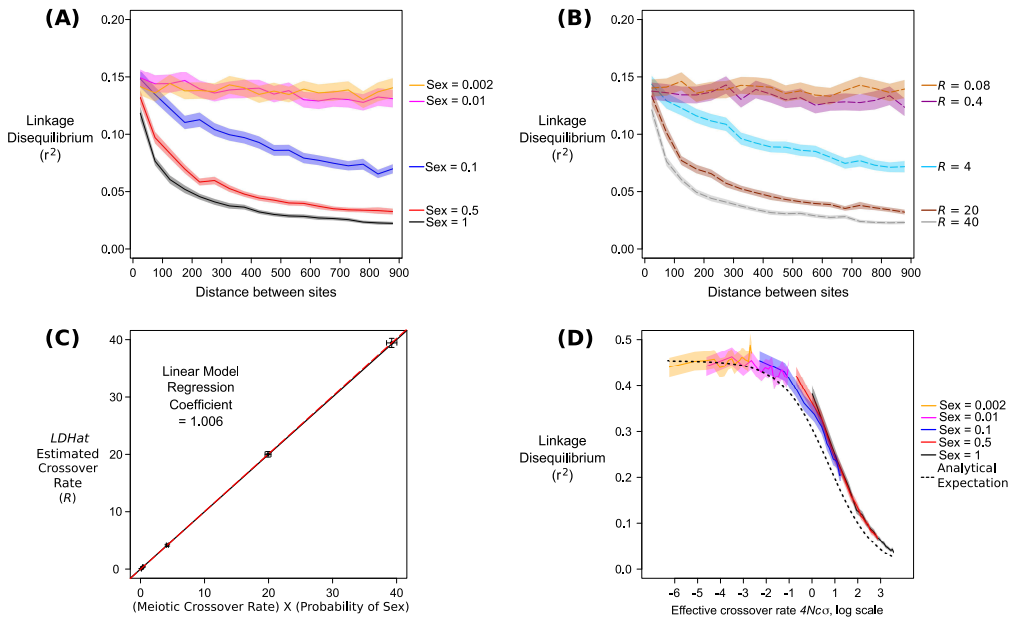


Figure 4: Effects of facultative, but not very low rates of sex (i.e. $\sigma \gg 1/N$) on estimates of meiotic crossing over. (a) Decay of linkage disequilibrium over 900 sites, as a function of distance between two sites. Different colours denote individual rates of sex, as shown in the legend. Solid line is the mean value over 1,000 simulations; fainter curves represent 95% confidence intervals. 50 paired samples were simulated (100 samples in total), $N = 10,000$, scaled mutation rate $\theta = 4N\mu = 10$, scaled crossover rate during sex $R = 40$. (b) As (a) but instead shows results from obligate sex simulations ran using `ms`, using a crossover rate equal to 40σ as shown in the legend. Due to binning of samples, r^2 is shown for distances between 25 to 875 sites apart in (a) and (b). (c) Estimates of R using `LDhat`, as a function of the ‘effective’ crossover rate used in the facultative-sex coalescent simulation. Points are mean estimates from 1,000 simulations, bars are 95% confidence intervals. Black line denotes $y = x$; dashed red line is the linear regression fit. (d) Plot of all simulation results in (a) but instead as a function of the rescaled recombination rate $4Nc\sigma$ (plotted on a natural log scale), and after omitting polymorphisms with minor allele frequency less than 10%. Dotted lines show analytical expectations (Equation 6). Note the different y-axis scale compared to panel (a).

430 disequilibrium when sex is low. Equation 7 captures the general behaviour of r^2
under low frequencies of sex (i.e., elevated r^2 values and a weaker dependence on
432 the meiotic crossover rate) but there are several reasons why the results do not
quantitatively match. Specifically, the analytical result is based on r_d^2 rather than
434 r^2 , and finite sample sizes also introduce additional complications ignored in the
calculation of expected r_d^2 . Our analytical model is intended to allow comparisons
436 of the main patterns with the comparable sexual model, rather than providing
precise predictions of the quantity as estimated by empiricists (which can instead
438 be calculated using the simulation).

Elevated r^2 occurs under low sex due to allelic sequence divergence creating
440 highly-differentiated haplotypes consisting of polymorphisms at intermediate fre-
quencies ($\sim 50\%$). These polymorphisms arise due to a lack of genetic segregation
442 creating highly differentiated haplotypes (Balloux *et al.* 2003; Bengtsson 2003;
Ceplitis 2003; Hartfield *et al.* 2016). Figure 5(b) shows the density of minor allele
444 frequencies over all simulation data, demonstrating that the $\Omega = 0.2$ case has many
sites with minor allele frequency between 45 and 50%. Consequently, r^2 is higher
446 over the genomic sample than expected based on obligate sex results using the ef-
fective crossover probability $c\sigma$. We also observe that linkage disequilibrium decay
448 is only weakly affected by the meiotic crossover frequency, in line with analytical
expectations (Equation 7).

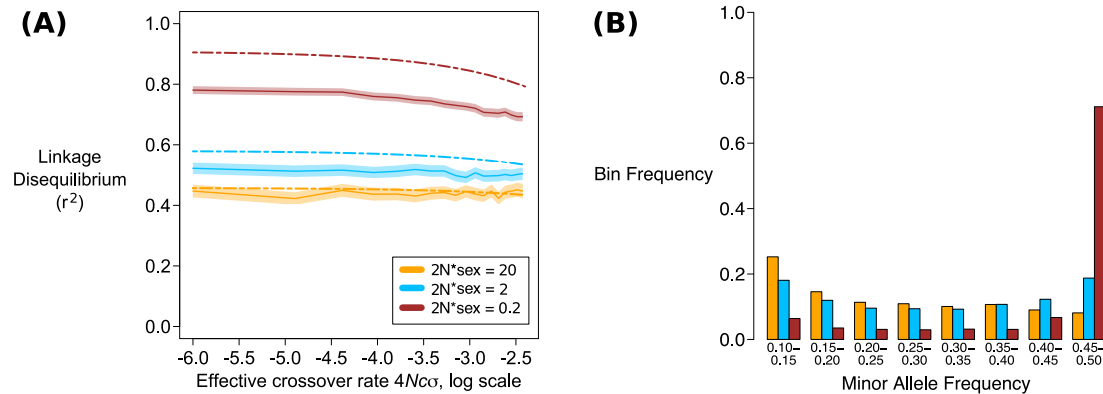


Figure 5: (a) Decay of linkage disequilibrium over 90,000 sites, as a function of the rescaled recombination rate $4Nc\sigma$ (on a natural log scale), and after omitting polymorphisms with minor allele frequency less than 10%. Different colours denote individual rates of sex, as shown in the legend. Solid line is the mean value over 1,000 simulations; fainter curves represent 95% confidence intervals. 50 paired samples were simulated (100 samples in total), $N = 10,000$, scaled mutation rate $\theta = 4N\mu = 10$, scaled crossover rate over all 100,001 sites $R\sigma = 0.1$. Coloured dash-dotted lines are low-sex analytical expectations for r_d^2 (Equation 7). r^2 is shown for distances between 2,500 to 87,500 sites apart. Results for short distances (125 to 4,375 sites apart) are shown in Figure E in Supplementary File S2. (b) Histogram of minor allele frequencies for the low-sex scenarios; the bin frequency is measured over all 1,000 simulations. Bar colours correspond to the same rates of sex as used in panel (a).

450 **Linkage disequilibrium with mitotic gene conversion**

High frequencies of sex

452 We ran simulations with mitotic gene conversion to investigate its effect on linkage disequilibrium. We define gene conversion using the population-level rate per sample, $\Gamma = 4Ng(L-1)$. We first ran simulations with no meiotic crossovers (i.e., some degree of sexual reproduction occurs, but not any meiosis-related processes); here, the decay of linkage disequilibrium is independent of the rate of sex (provided sex is not too low; Figure 6(a)). This decay is similar to that observed in obligate sexual populations experiencing the same gene conversion rate (Figure 6(b)). When meiotic crossovers are included with rate $R = 40$, disequilibrium profiles 460 separate out depending on the frequency of sex (Figure 6(c)), and are similar to those arising in obligate sexuals that experience the same gene conversion rate and an effective crossover probability $c_{eff} = c\sigma$ (Figure 6(d)). The pattern of linkage disequilibrium decay is more dependent on the probability of sex when the 464 frequency of mitotic gene conversion is low, relative to the crossover probability c (contrast Figure 6 that uses $\Gamma = 20$, with Figure F in Supplementary File S2 that uses $\Gamma = 2$).

Low frequencies of sex

468 With low frequencies of sex ($N\sigma \leq \mathcal{O}(1)$), within-individual diversity is affected by the ratio of sex to gene conversion at a site, denoted ϕ (Hartfield *et al.* (2016); ϕ is defined mathematically below). If sex occurs more frequently than gene conversion 470 ($\phi > 1$), elevated within-individual diversity should be observed. However, if gene conversion arises at the same frequency, or more often than sex ($\phi \leq 1$), then gene 472

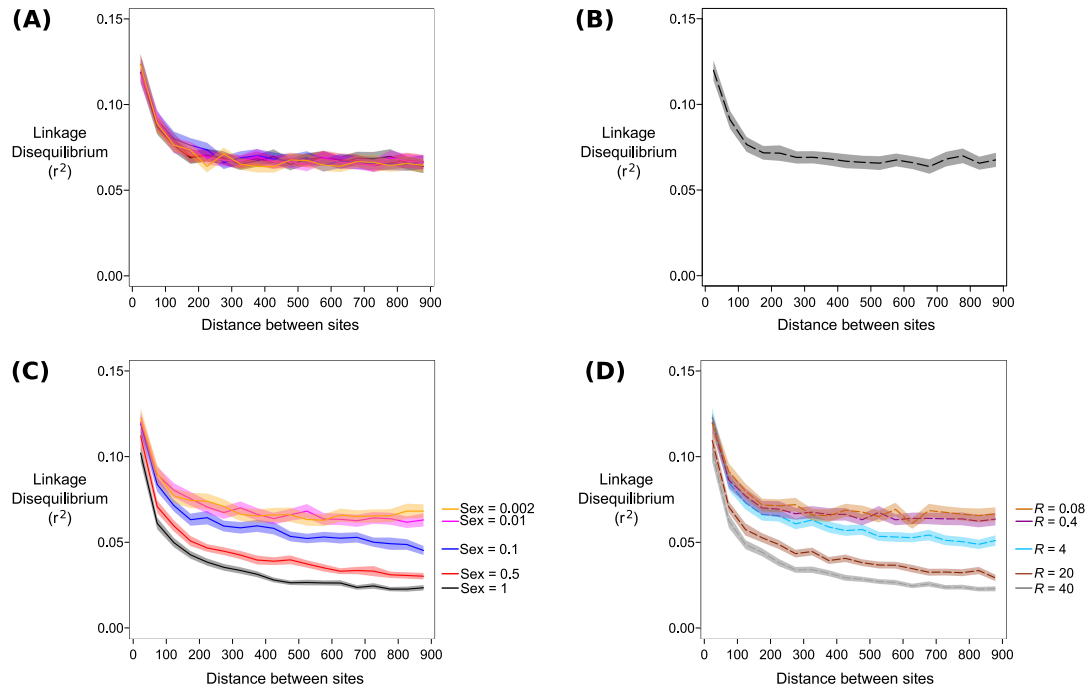


Figure 6: Decay of linkage disequilibrium over 900 sites, as a function of distance between two sites as caused by mitotic gene conversion with high rates of sex ($\sigma \gg 1/N$). 50 paired samples are taken from a population of size $N = 10,000$, scaled mutation rate $\theta = 10$, and mitotic gene conversion occurs with rate $\Gamma = 20$ (with average gene conversion tract length $\lambda = 100$ sites). Meiotic crossovers are either (a, b) absent or (c, d) present at rate $R = 40$. (a, c) Results from the facultative-sex coalescent simulation with different probabilities of sex. Colours are as shown in the legend; shaded bands are 95% confidence intervals. (b, d) Results from *ms* with 100 samples and the same gene conversion rate, with crossover probability $c_{eff} = c\sigma$ in (d). Note only one *ms* comparison is plotted in (b). Equivalent results with $\Gamma = 2$ are shown in Figure F in Supplementary File S2. r^2 is shown for distances between 25 to 875 sites apart.

conversion will lead to reduced within-individual diversity compared to a sexual
474 population (Hartfield *et al.* 2016, Eq. 11). Hence we next ran simulations with
different ϕ values to explore the relative effects of both phenomena on linkage
476 disequilibrium.

We considered a diploid population $N = 10,000$ from which we simulated 50
478 paired samples; $\theta = 10$; and a genetic segment that is $L = 10,001$ sites long.
To focus on the effects of gene conversion, we assumed no meiotic crossing over
480 and only mitotic gene conversion was considered, with events having a mean tract
length of $\lambda = 1,000$ sites, matching estimates of non-crossover events obtained
482 from yeast (Judd and Petes 1988; Martini *et al.* 2011). We fixed $\Omega = 2N\sigma = 2$
and varied Γ so that the ratio $\phi = (\Omega Q)/\Gamma$ (for $Q = (L - 1)/\lambda$ the number of
484 breakpoints in units of mean gene conversion length), which determines neutral
diversity at a single site, equals either 10, 1 or 0.1 (requiring $\Gamma = 2, 20$ and 200
486 respectively). Note that we define the probability of gene conversion per haplotype
rather than per diploid genotype, so the probability of gene conversion is scaled
488 by $4N$ as opposed to the $2N$ scaling used in Hartfield *et al.* (2016) (i.e., there is
an extra factor of 2 in the denominator of ϕ to account for two haplotypes per
490 individual).

Figure 7(a) demonstrates the unusual behaviour associated with high gene
492 conversion with low rates of sex, with r^2 being a non-monotonic function of the gene
conversion frequency, in line with analytical findings (Figure 3(c)). Mitotic crossing
494 over at rate $\rho_A = 4N\tilde{c}_A(L-1) = 10$ breaks down linkage disequilibrium over longer
distance for $\Gamma = 2$ and 20, but not for $\Gamma = 200$ (Figure 7(b)). Both results are
496 in line with analytical findings: r^2 is a non-monotonic function of gene conversion
when sex is rare (Figure 3(c)), and the presence of mitotic recombination can

498 reduce long-distance r^2 , unless mitotic gene conversion acts at a much higher rate
(Figure 3(d)).

500 Elevated linkage disequilibrium is likely related to the reduced mean coales-
cence times that arise under frequent gene conversion. To further understand this
502 behaviour, we can relate the observed r^2 values to Equation 11 of McVean (2002),
which demonstrated how r_d^2 can be written as a function of both the correlation
504 in coalescent times between sites, and the ratio of the mean coalescent time to the
variance:

$$r_d^2 = \frac{Corr[ij, ij] - 2Corr[ij, ik] + Corr[ij, kl]}{(E[\tau]^2/Var[\tau]) + Corr[ij, kl]} \quad (8)$$

506 $Corr$ in Equation 8 represent correlation in coalescent times between pairs of
sites (e.g., $Corr[ij, kl]$ the correlation in coalescence times where site one is taken
508 from haplotype i and j , and site two is taken from haplotype k and l). $E[\tau]$ and
 $Var[\tau]$ are the mean and variance of coalescent times. Equation 8 shows that r_d^2 is
510 not just reduced with lower covariances between pairs of loci, but it also decreases
with higher $E[\tau]^2/Var[\tau]$. This ratio equals one under the standard coalescent,
512 but low sex alters the mean and variance of coalescent times (Hartfield *et al.* 2016)
which will also affect this ratio, and subsequently alter linkage disequilibrium val-
514 ues. Figure 7(c) plots the covariance in coalescent times over all simulations, for
two sites sampled from a single individual. We see that they are consistently lower
516 with higher rates of gene conversion, reflecting how genetic material is more fre-
quently transferred between samples. We next looked at the ratio $(E[\tau]^2/Var[\tau])$,
518 which can be calculated from Equations 11 and 12 of Hartfield *et al.* (2016). We
focussed on the within-individual coalescence times, as these are directly affected

520 by within-individual mitotic gene conversion. This ratio is shown in Figure 7(d)
for $\Omega = 2$ as a function of the mitotic gene conversion rate for a single site, Γ_1 . As
522 Γ_1 increases, the ratio ($E[\tau]^2/Var[\tau]$) decreases, leading to the observed increase
in r^2 (Figure 7(d)). This result suggests that high rates of within-individual gene
524 conversion distorts underlying genealogies, so that observed linkage disequilibrium
is higher than that expected based on the rate of gene exchange alone. In contrast,
526 meiotic crossing over has no direct effect on this ratio.

In Supplementary File S2 we investigate how linkage disequilibrium is affected
528 if we alter g and λ while fixing the product $g\lambda$. Linkage disequilibrium decays
more rapidly for higher g values with lower λ as there are more gene conversion
530 events that break apart coalescent histories between individual sites.

Effect of Population Subdivision

532 Measurements of linkage disequilibrium are known to increase under population
structure with obligate sex (Wakeley and Lessard 2003), as polymorphisms that
534 only appear in specific regions will naturally be in disequilibrium, increasing r^2 .
Facultatively sexual organisms are known to show strong geographic differentiation
536 (Arnaud-Haond *et al.* 2007). Hence we examined the effects of population structure
in facultatively sexual organisms. We assumed an island model, consisting of 4
538 demes with a scaled migration rate $M = 2N_T m$ between them (for $N_T = 10,000$
the total population size across all demes). 50 paired samples were simulated,
540 with 13 samples taken from two demes, and 12 from the other two. Population-
scaled parameters are subsequently defined relative to N_T (i.e., $R = 4N_T \tilde{c}(L - 1)$,
542 $\Omega = 2N_T \sigma$, $\Gamma = 4N_T g(L - 1)$).

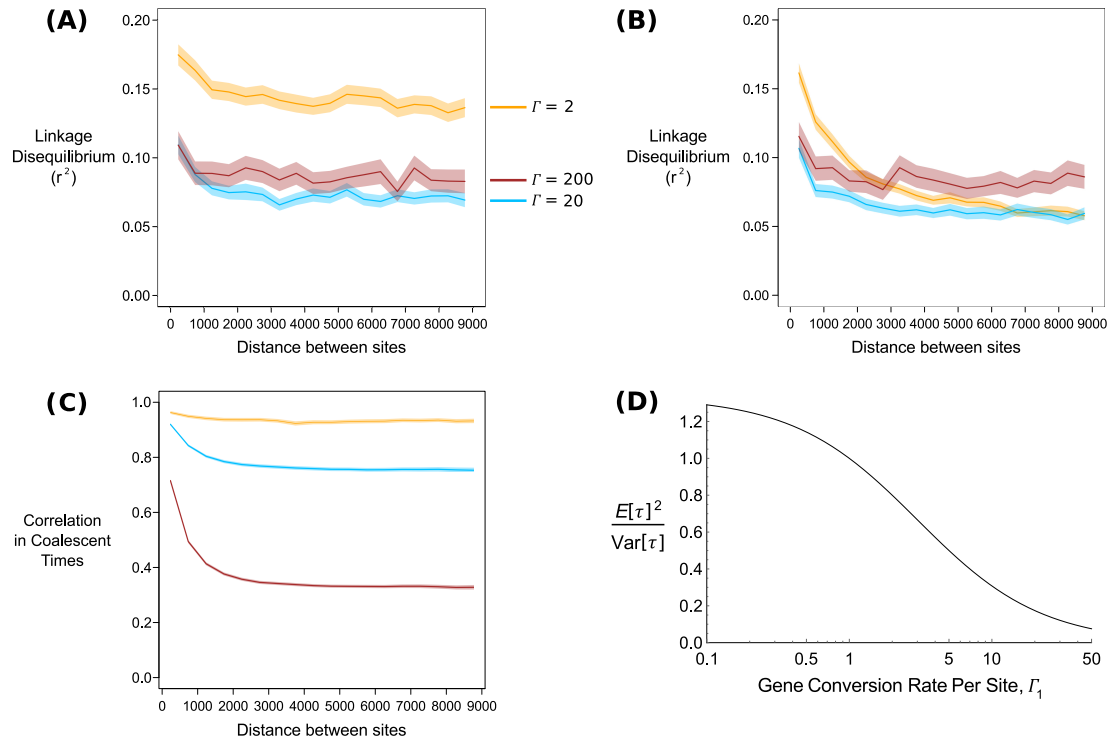


Figure 7: (a) Plot of linkage disequilibrium, measured using r^2 , as a function of distance between two sites. For a fixed rate of sex $\Omega = 2$, gene conversion is set to $\Gamma = 2$ (orange line); 20 (blue line); or 200 (red line) with $\lambda = 1,000$. Shading around lines indicate 95% confidence intervals. (b) As (a) but also including mitotic recombination with rate $\rho_A = 4N(c_A) = 10$. Results over short distances for (a) and (b) (25 to 875 sites apart) are presented in Figure G in Supplementary File S2. (c) Correlation in coalescent times ($Corr[ij, ij]$ in Equation 8) between sites for the three Γ values, assuming no mitotic crossing over (i.e., $\rho_A = 0$). Note that for $\Gamma = 20$ and 200, confidence intervals are only slightly thicker than the mean line. (d) Ratio of $(E[\tau]^2 / \text{Var}[\tau])$ for two samples taken from the same individual, as a function of the scaled gene conversion rate per site Γ_1 , with $\Omega = 2$. (a)–(c) are shown for distances between 250 to 8,750 sites apart.

For high sex cases ($\sigma \gg 1/N_T$), and low sex cases ($N_T\sigma \leq \mathcal{O}(1)$) where mitotic
544 gene conversion is present, results are qualitatively similar to those observed for
a single population (Supplementary File S2). For the low-sex case with meiotic
546 crossing-over, we ran simulations with $R\sigma = 0.1$ and Ω equal to 20, 2 or 0.2, and
compared them to an obligate sex case with the same crossover rate with differ-
548 ent rates of migration. With high migration ($M = 10$) the results are similar to
what is observed without population structure, with disequilibrium visually de-
550 caying along the genome sample for $\Omega = 0.2$. Yet values are lower than in the
panmictic case (compare the red line in Figure 8(a) with Figure 5). With lower
552 migration ($M = 0.1$), disequilibrium values are unexpectedly reduced as the prob-
ability of sex decreases (Figure 8(b)). The reason for this unintuitive result is
554 due to the partitioning of low-frequency polymorphisms under both low sex and
population structure. With low migration rates, strong population structure is
556 present so polymorphisms are localised to specific demes. Low frequencies of sex
further partition polymorphisms within demes on diverged haplotypes (Figure 5(e)
558 in Hartfield *et al.* (2016)). Hence the presence of rare sex, alongside high popu-
lation structure, creates more polymorphisms at lower frequencies compared to
560 populations with higher probabilities of sex (Figure 8(c, d)). These polymorph-
isms tend to have small values for r^2 , thereby reducing the average value. After
562 removing polymorphisms with minor allele frequency less than 15%, estimates of
 r^2 become similar for all rates of sex, although $\Omega = 0.2$ results are still slightly
564 lower than other cases for $M = 0.1$ (Figure J in Supplementary File S2).

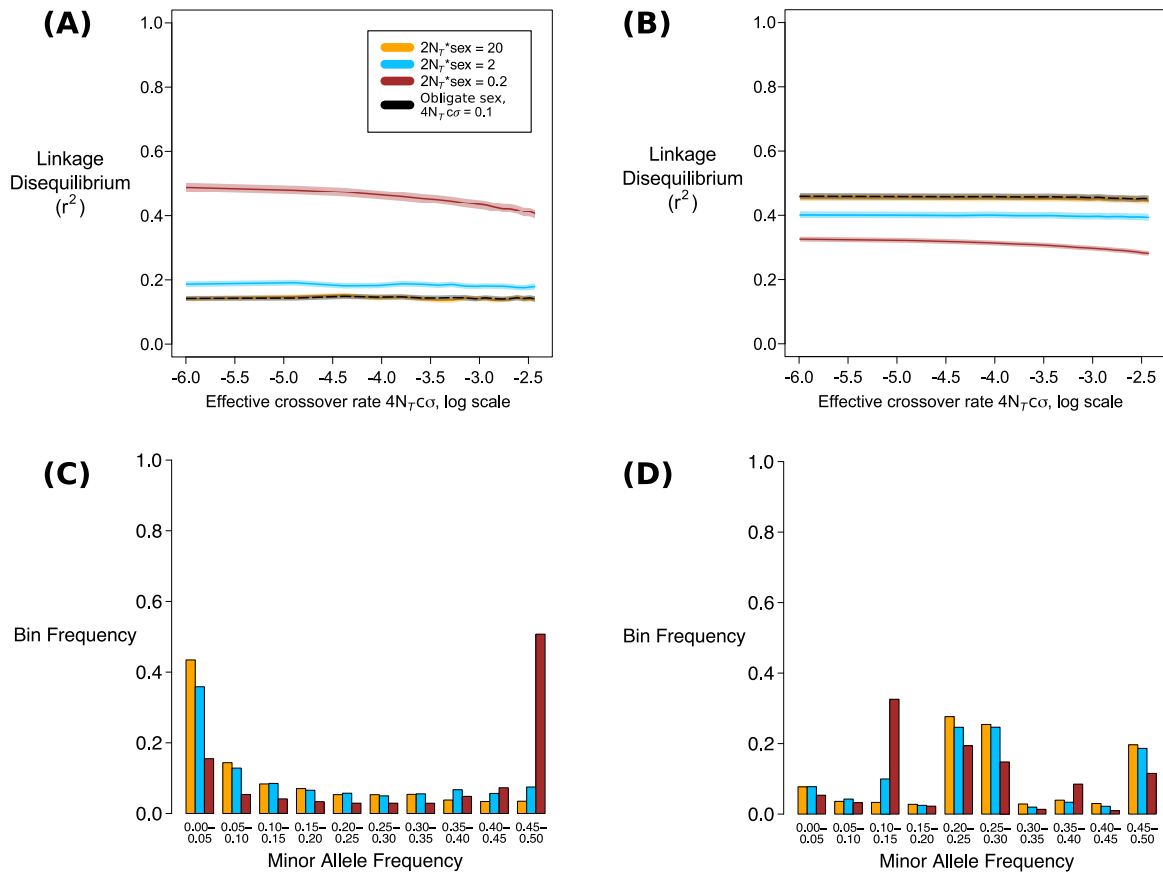


Figure 8: (a, b) Decay of linkage disequilibrium over 90,000 sites from samples taken over a subdivided population, as a function of the rescaled recombination rate $4N_T c \sigma$ (plotted on a natural log scale). Different colours denote individual rates of sex, as shown in the legend. Solid line is the mean value over 1,000 simulations; fainter curves represent 95% confidence intervals. 50 paired samples were simulated (100 samples in total) over 4 demes, $N_T = 10,000$, scaled mutation rate $\theta = 4N_T \mu = 10$, scaled crossover rate over entire ancestral tract $R\sigma = 0.1$, scaled migration rate is either (a) $M = 10$ or (b) $M = 0.1$. Black dashed line is equivalent obligate sex simulation ran using `ms` with 100 samples. r^2 is shown for distances between 2,500 to 87,500 sites apart. (c, d) Histogram of minor allele frequencies, with the bin frequency measured over all 1,000 simulations. Bar colours correspond to the same rates of sex as used in panels (a, b).

Discussion

566 Summary of results

Existing single-locus theory for facultatively sexual organisms shows behaviour distinct from sexual cases only with extremely low frequencies of sex ($\sigma \leq \mathcal{O}(1/N)$; Bengtsson (2003); Ceplitis (2003); Hartfield *et al.* (2016)). In this paper we provide novel analytical and simulation results to investigate how correlations in genetic diversity across loci are affected by facultative sex. We also provide an updated version of a simulation package, and explain how existing crossover (Hudson 1983) and multi-site gene conversion routines (Wiuf and Hein 2000) can be included in facultative-sex coalescent processes, to investigate how they affect gene genealogies. This program can be used to simulate ancestral recombination graphs of facultatively sexual organisms.

When the frequency of sex is high ($N\sigma \gg 1$), we observe that the breakdown in linkage disequilibrium in a genetic sample is similar to that observed in an obligate sex model using an effective crossover probability $c_{eff} = c\sigma$ (Figure 3(a), Figure 4). This result reflects similar behaviour in partially self-fertilising organisms (Nordborg 2000), where the effective crossover rate is equal to $r(1 - F)$ for F the inbreeding rate (although this scaling breaks down with high self-fertilisation and crossover rates; Padhukasahasram *et al.* (2008); Roze (2009, 2016)).

Hence if there exists knowledge of meiotic crossover rates, then one can use linkage disequilibrium data to estimate the overall frequency of sex. The situation becomes more complicated if mitotic recombination is present as it also breaks down linkage disequilibrium, even under low frequencies of sex. If sex is frequent but crossing over is rare, mitotic gene conversion principally affects linkage dis-

equilibrium (Figure 6(a)). Once crossing-over probabilities become high then these
590 principally break down linkage disequilibrium, so the effective crossover rate scal-
ing $c_{eff} = c\sigma$ still holds (Figure 6(b)).

592 When rates of sex become low ($\sigma \leq \mathcal{O}(1/N)$), the decay in linkage disequi-
librium can no longer be captured by rescaling $c_{eff} = c\sigma$, as the distribution
594 of genealogies becomes fundamentally different than when sex is common (Fig-
ure 3(b-d)). In the absence of gene conversion, r^2 becomes elevated with low rates
596 of sex, reflecting more linked polymorphisms present at intermediate frequencies
(Figure 5). If mitotic gene conversion is present, the ratio between rates of sex and
598 gene conversion ϕ becomes a strong determinant of linkage disequilibrium, with
unexpected behaviour arising if gene conversion occurs at high rates relative to
600 sex. Increasing gene conversion will first reduce overall disequilibrium values due
to gene exchange breaking down associations between sites. Yet very high rates
602 of gene conversion then cause elevated linkage disequilibrium values, which is a
consequence of how gene conversion changes the distribution of coalescence times.
604 Adding mitotic crossovers reduces the minimum observed linkage disequilibrium,
unless mitotic gene conversion occurs at much higher rates (Figures 3(c, d) and
606 7). Finally, low sex combined with low migration rates in subdivided populations
also reduces r^2 values, due to more low-frequency polymorphisms being present
608 within demes (Figure 8). These non-intuitive effects illustrate the value of expli-
cantly modelling genetic diversity under low rates of sex when considering genomic
610 data for facultatively sexual organisms.

Future Directions

612 The creation of the new coalescent algorithm that accounts for facultative sex,
crossing over and gene conversion can be used as a basis for inferring these pro-
614 cesses from genomic data. This can be achieved by using coalescent simulations
to create likelihood profiles over two loci (Hudson 2001; McVean *et al.* 2002; Wall
616 2004; Auton and McVean 2007). An alternative approach would be to use Ap-
proximate Bayesian Computation to recurrently simulate different outcomes, each
618 time comparing them to the real data and keeping those that match sufficiently
well, to build a pseudo-likelihood (Sunnåker *et al.* 2013). Simulation results also
620 suggest that it is important to jointly consider both genome-wide diversity and
linkage disequilibrium if we wish to infer the effects of sex, meiotic crossovers, and
622 gene conversion, especially if mitotic gene conversion is pervasive (Figure 7).

We anticipate that the *FacSexCoalescent* simulation can be expanded upon in
624 the future to account for more complex scenarios. The only population structure
we considered is an island model, whereas bottlenecks or unequally-sized subpopu-
626 lations are common (Pool and Aquadro 2006; Veeramah and Hammer 2014; Frantz
et al. 2016). The gene conversion model can also be expanded upon to consider
628 context-dependent events (for example, GC-biased gene conversion; Duret and
Galtier (2009)). Given ongoing debates on how gene conversion potentially affects
630 genetic diversity and fitness in facultatively sexual organisms (Mancera *et al.* 2008;
Flot *et al.* 2013; Tucker *et al.* 2013), a deeper understanding of how gene conver-
632 sion affects the distribution of genetic diversity can shed further insight into what
processes influence genetic evolution in facultatively sexual organisms.

634 **Acknowledgements.** We would like to thank two anonymous reviewers and

Associate Editor John Wakeley for providing constructive comments on the ma-
nuscript. MH was supported by a Marie Curie International Outgoing Fellow-
636 ship, grant number MC-IOF-622936 (project SEXSEL), and an European Research
Council grant (FP7/20072013, ERC Grant 311341) awarded to Thomas Bataillon.
638 This work was also supported by Discovery Grants (AFA & SIW) from the Natural
640 Sciences and Engineering Research Council of Canada.

A Implementing Recombination into the Facultative Sex Simulation Algorithm

Overview of basic coalescent simulation

644 Here we outline the implementation of meiotic and mitotic recombination events in the facultative sex coalescent simulation routine (Hartfield *et al.* 2016). We describe the probability that set events occur per generation; that is, both the time in the past to the next event and resolution of events are based on unscaled probabilities (as opposed to rates, where a probability is multiplied by the population size to give the expected number of events per generation). We define p_{NS} as the probability that none of the x paired samples are split by sex and p_{E0} as the probability of any event (e.g., coalescence, recombination) given that none of the paired samples are affected by sex. The absolute time to the next event is drawn from a geometric distribution with parameter $p_{sum} = (1 - p_{NS}) + p_{NS}p_{E0}$; this time is rescaled by $2N$ so that it is on a coalescent timescale. It is subsequently determined whether any and, if so, how many of the x paired samples segregate into different individuals due to sexual reproduction. If k of x paired samples are produced via sex, then $2k$ new unpaired samples are created. The total probability of any other event occurring is then re-calculated, conditional on this updated sample configuration. It is determined whether any such event occurs, and which type if one does arise; the sample configuration is updated appropriately. Note that if sex is common, the first term in p_{sum} is large and all paired samples are rapidly split by sex, so the model then behaves like a haploid process. If the population is structured as an island model, the logic is similar but we instead track x_i ,

664 y_i paired and unpaired haplotypes in deme i , and consider $2N_T$ total haplotypes
over all subpopulations. We refer the reader to Hartfield *et al.* (2016) for further
666 details of the basic coalescent simulation.

Implementing Meiotic and Mitotic Crossing Over

668 We outline the probability of either a crossover or gene conversion event occurring
each generation, then implement these probabilities into the calculation of p_{sum}
670 as described above. As with the single-locus routines, we assume that sexual re-
production occurs first, followed by subsequent gene exchange events. Let \tilde{c} be
672 the absolute meiotic crossover probability between any two adjacent sites, condi-
tional on sex having occurred; \tilde{c}_A the mitotic crossover probability (which is not
674 conditional on the reproductive mode); and L the number of sites that the genetic
samples cover. Assuming \tilde{c} and \tilde{c}_A are small, the total meiotic crossover probability
676 in each individual at the start of the process is $\tilde{c}(L-1)$. We assume that the total
recombination probability is low (i.e., $\tilde{c}(L-1), \tilde{c}_A(L-1) \sim \mathcal{O}(1/N)$) so we do not
678 consider outcomes where more than one crossover event occurs per generation.

Following sexual reproduction, crossovers act on unpaired samples with prob-
680 ability $(\tilde{c} \sigma + \tilde{c}_A)L_{e,y}$. The quantity $L_{e,y}$ is the ‘effective’ crossover length summed
over all y unpaired samples. We include this term to ensure that unnecessary cros-
682 sover events are not considered, thus speeding up the routine (Hein *et al.* 2005).

$L_{e,y}$ is defined as follows: let $L_{s,i}$ be the first ancestral site in unpaired sample i ,
684 and $L_{t,i}$ the last ancestral site. Then $L_{e,i} = L_{t,i} - L_{s,i}$ equals the total number of
breakpoints where a crossover can create two new samples, each carrying ances-
686 tral material; note that any sites within individual haplotypes that have reached

their most recent common ancestor are converted into non-ancestral material (Hein
688 *et al.* 2005). Then $L_{e,y} = \sum_{i \in y} L_{e,i}$. This crossover event creates two new samples,
with each part carrying ancestral material (Figure 1(a)).

690 If k out of the x paired samples segregate via sex into $2k$ new unpaired samples,
then the crossover probability is increased by adding on an extra $(\tilde{c} + \tilde{c}_A)L_{e,2k}$ term.
692 Here $L_{e,2k}$ is the ‘effective’ crossover length over the $2k$ new unpaired samples,
defined in a similar manner to $L_{e,y}$. The $2k$ samples are a transitory class of un-
694 paired haplotypes, created through sexual reproduction segregating paired samples
into distinct individuals (see also Figure 1(b, c)). Because they are already determ-
696 ined to have been created by sex by an earlier step in the algorithm, there is
no factor σ contributing to their probability of experiencing meiotic crossing over.
698 Those that do not undergo crossing-over become regular unpaired samples (Fig-
ure 1(b)); those that do are transformed into regular paired samples (Figure 1(c)).

700 Mitotic crossing over can act on the remaining $x - k$ paired samples that do
not undergo sexual reproduction. This event occurs with probability $\tilde{c}_A L_{e,x-k}$, for
702 $L_{e,x-k}$ the effective crossover length measured over both arms within the remaining
 $x - k$ paired samples. $L_{e,x-k}$ is measured in a different manner than for unpaired
704 samples. Let i be an individual where both haplotypes i_1, i_2 are sampled. Define
 L_{s,i_1}, L_{s,i_2} as the first ancestral site in each of these samples, and L_{t,i_1}, L_{t,i_2} the
706 last ancestral sites. Then the first ancestral site at which mitotic crossing over
is valid in individual i is $L_{s,i} = \min(L_{s,i_1}, L_{s,i_2})$; similarly, $L_{t,i} = \max(L_{t,i_1}, L_{t,i_2})$.
708 Then $L_{e,i} = L_{t,i} - L_{s,i}$ and $L_{e,x-k} = \sum_{i \in (x-k)} L_{e,i}$. Mitotic crossing over exchanges
genetic material between the two samples within an individual (Figure 1(d)).

710 These probabilities are considered alongside other events to determine whether
the next event involves a meiotic crossover. If it is chosen, then one of the appro-

712 priate samples is picked at random (weighing by the length of extant breakpoints
present in each sample), and the appropriate outcome is enacted. Note that if the
714 potential for crossing over is high (i.e. if the probability of sex and crossing over is
high, and there are a large number of samples) then the net recombination prob-
716 ability can exceed one, as the assumption that only up to one recombination event
occurring per generation is violated, causing the algorithm to terminate. Hence
718 large crossover probabilities should be avoided.

Implementing Meiotic, Mitotic Gene Conversion

720 To account for both meiotic and mitotic gene conversion events (Figure 1(e-g)), up
to four additional parameters are specified. Two new parameters are g_S and g , the
722 probabilities of either meiotic or mitotic gene conversion occurring with its leftmost
boundary arising on the recipient homolog at a given site. We also define the
724 average length of gene conversion events, denoted λ_S for meiotic gene conversion
and λ for mitotic gene conversion. We implement and extend the algorithm of Wiuf
726 and Hein (2000) to calculate the probability of either type of gene conversion event
occurring each generation. Here, the length of gene conversion events (scaled by
728 the total number of breakpoints) is drawn from an exponential distribution with
parameter $Q = (L - 1)/\lambda$, the number of breakpoints in units of average gene
730 conversion length (Wiuf and Hein 2000). We define distinct $Q_S = (L - 1)/\lambda_S$,
 $Q = (L - 1)/\lambda$ for meiotic and mitotic gene conversion events. Further details
732 of the mathematical derivations are in Section B of Supplementary Mathematica
File S1.

734 There also exists a special class of gene conversion events, where conversion

initiates outside the ancestral tract and extends completely over ancestral material
736 (Figure 1(h)). If there exist $x - k$ pairs after k of them are split by sex, then
the probability of this event happening equals $2(x - k)(g(L - 1)e^{-Q})/Q$ (a full
738 derivation is presented in “Deriving probability of ‘complete’ gene conversion”
below, and Section C of Supplementary Mathematica File S1).

740 **Determining type of gene conversion (meiotic or mitotic)**

To understand how the different events (meiotic and mitotic gene conversion)
742 are considered, it is easiest to relate calculations to the obligate sex case with a
single type of gene conversion event. Here, the product of the gene conversion
744 probability g_0 (using g_0 to differentiate this general gene conversion probability
from the mitotic gene conversion notation) and the number of breakpoints $L - 1$
746 is such that $g_0(L - 1) \sim \mathcal{O}(1/N)$. Then the probability of a disruptive gene
conversion event in a sample of length L is $g_0(L - 1)Q_0^*$, where g_0 is the probability
748 that the leftmost edge of a gene conversion tract is at a given site, and:

$$Q_0^* = 1 + \frac{1}{Q_0} (1 - e^{-Q_0}) \quad (\text{A1})$$

$Q_0 = (L - 1)/\lambda_0$ is the number of breakpoints in units of average gene conversion
750 length (here too, we use Q_0 , Q_0^* and λ_0 to define this general gene conversion
process). Q_0^* accounts for gene conversion events that only partly lie in ancestral
752 material (i.e., only one end of the gene conversion lies in ancestral material) as
well as those that lie entirely within this region (i.e., both breakpoints lie within
754 ancestral material). Equation A1 assumes that the length of gene conversion
events (scaled by the total number of breakpoints) is drawn from an exponential

756 distribution with parameter Q_0 (Wiuf and Hein 2000). Equation A1 also disregards
possible edge effects (e.g., if the ancestral tract lies near the chromosome edge).
758 In the facultative-sex coalescent, we can partition this probability depending on
the type of conversion event (meiotic or mitotic), and the number of each type
760 of sample (paired or unpaired) present at the time. Let there be $(x - k)$ paired
samples after k of them have split after sex, making $2(x - k)$ haplotypes in total;
762 y unpaired samples; and $2k$ new unpaired samples following genetic segregation.
After partitioning over all possible outcomes, the total probability of disruptive
764 gene conversion equals:

$$\Sigma = 2Q^*g(L-1)(x-k) + y(Q^*g(L-1) + \sigma Q_S^*g_S(L-1)) + 2k(Q^*g(L-1) + Q_S^*g_S(L-1)) \quad (\text{A2})$$

Here, Q^* and Q_S^* are equal to Q_0^* above, with parameters $Q = (L - 1)/\lambda$
766 and $Q_S = (L - 1)/\lambda_S$ for mitotic and meiotic gene conversion respectively. As
segregation has already been resolved, the $(x - k)$ remaining paired samples repro-
768 duce asexually so only they can be subject to mitotic gene conversion. Unpaired
samples can be subject to both meiotic and mitotic gene conversion, hence for
770 each unpaired sample (y in total) we also have to consider the probability of sex
 σ . Note that there is no σ term when considering the $2k$ new unpaired samples, as
772 they have already undergone sex by this point in the algorithm. In contrast to the
crossover procedure, we do not weigh samples by the number of breakpoints within
774 ancestral material; gene conversion events affecting only non-ancestral material are
allowed to occur.

776 When a disruptive gene conversion event occurs, it is first determined if it acts

on unpaired or paired samples. The probability that gene conversion acts on a
778 paired sample is $2Q^*g(L-1)(x-k)/\Sigma$ where Σ is given by Equation A2, and one
minus this probability is the chance it acts on unpaired samples. If acting on a
780 paired sample then only mitotic gene conversion can occur. If acting on unpaired
samples, a further random draw is made to determine whether the gene conversion
782 event is meiotic or mitotic. Let $\Upsilon = g(L-1)Q^*(y+2k) + g_S(L-1)Q_S^*(y\sigma+2k)$ be
the probability of a gene conversion event that occurs on an unpaired sample. If
784 an unpaired sample undergoes conversion, the probability that the event is mitotic
equals $(g(L-1)Q^*(y+2k))/\Upsilon$; a similar calculation can be made for meiotic gene
786 conversion.

Drawing start, end breakpoints following gene conversion

788 The scaling terms Q^* , Q_S^* account for the fact that gene conversion does not
necessarily take place entirely within the gene tract, but may only partially overlap
790 with it. We follow the logic outlined in Wiuf and Hein (2000) to accurately model
the relative frequency of each of these events. Given the tract length in units of
792 conversion events Q_0 (which can be either Q or Q_S), $K(Q_0) = 1 - (1 - \exp(-Q_0))/Q_0$
is the probability that if gene conversion starts in the sample, it will also end within
794 it (Wiuf and Hein 2000, Eq. 2). One can then define the probability that both
breakpoints occur within the sample (Wiuf and Hein 2000, Eq. 11):

$$p_2 = \frac{K(Q_0)}{2 - K(Q_0)} \quad (\text{A3})$$

796 The probability that only one breakpoint falls within the sample equals $p_1 =$
 $1 - p_2$ (Wiuf and Hein 2000, Eq. 12). We first choose whether one or both

798 breakpoints lie within the sample, as determined by Equation A3. The appropriate
start and end points are then chosen from the relevant probability distributions.
800 Wiuf and Hein (2000) determined how the distribution of breakpoints depends on
whether one or both breakpoints lie within the genome tract. For example, if only
802 one breakpoint lies in the tract then it is likelier to occur closer to one of its edges.
When choosing gene conversion breakpoints, they are selected by calculating the
804 cumulative distribution function (CDF) for the event; drawing an initial start or
end point from a uniform distribution; then plugging this uniform draw into the
806 inverse CDF to obtain the true start or end point. The CDFs are obtained from the
relevant probability distribution functions outlined by Wiuf and Hein (2000). Note
808 that the resulting outputs are continuous variables lying between 0 and 1, while
the simulation program assumes discrete breakpoints. Hence after the relevant
810 breakpoint locations have been found, it is then converted into the appropriate
discrete value lying between 1 and $L - 1$, including these values. Further details on
812 the following derivations are provided in Section B of Supplementary Mathematica
File S1.

814 If *two breakpoints are chosen*, then the joint probability distribution of start
points s and end points t equals $f(s, t) = (Q_0 \exp(-Q_0(t - s)))/K(Q_0)$ (Wiuf and
816 Hein 2000, Eq. 4). By integrating out t from s to 1, one obtains the marginal
density of start points, $f(s) = (1 - \exp(-Q_0(1 - s)))/K(Q_0)$ (Wiuf and Hein 2000,
818 caption of Fig. 4). The CDF of s can then be calculated as:

$$F(S) = \int_0^S f(s) = \frac{1 - e^{Q_0 S} + e^{Q_0} Q_0 S}{1 + e^{Q_0} (Q_0 - 1)} \quad (\text{A4})$$

To choose a start point, we draw a value between 0 and 1 from a uniform

820 distribution and plug it into $F^{-1}(S)$, which equals:

$$F^{-1}(S) = \frac{e^{-Q_0}}{Q_0} \cdot (S - 1 + e^{Q_0}((Q_0 - 1)S - W[-e^{-Q_0 - e^{-Q_0}(1-S) - (1-Q_0)S}]))) \quad (\text{A5})$$

where W is the Lambert function (Abramowitz and Stegun 1970). To draw the
822 respective end point, we first need to determine the distribution $f(t|s)$; i.e., the
density of end points *given* a starting point s . This function is also equal to
824 $f(s, t)/f(s) = (Q_0 \exp(-Q_0(t - s)))/(1 - \exp(-Q_0(1 - s)))$. From this function
we obtain the CDF of T given s , as well as the inverse CDF:

$$F(T|s) = \int_s^T f(t|s) = \frac{1 - \exp(-Q_0(T - s))}{1 - \exp(-Q_0(1 - s))} \quad (\text{A6})$$

$$F^{-1}(T|s) = s - \frac{\log(1 - T(1 - \exp(-Q_0(1 - s))))}{Q_0} \quad (\text{A7})$$

826 Equation A7 is then used to determine the endpoint of of the gene conversion
event, which automatically lies within the length of the genetic sample. If the
828 chosen endpoint is the same as the startpoint, then another endpoint is chosen so
that they are distinct.

830 If *one breakpoint is chosen*, it can be the start or end of gene conversion with
equal probability (Wiuf and Hein 2000, Eq. 7). If it is chosen to be the end
832 point of gene conversion initiating outside the tract, then the start point is set to
zero (i.e., the far left edge of the tract). The probability density of end points t
834 is $f(t) = \exp(-Q_0 t)/(1 - K(Q_0))$ (Wiuf and Hein 2000, Eq. 8). This function
is left-skewed; end points are likely to be near the left-hand side of the genetic

836 sample. The CDF and inverse CDF can be calculated as:

$$F(T) = \frac{\exp(Q_0) - \exp(Q_0(1 - T))}{\exp(Q_0) - 1} \quad (\text{A8})$$

$$F^{-1}(T) = 1 - \frac{\log(\exp(Q_0) + T - \exp(Q_0T))}{Q_0} \quad (\text{A9})$$

If the single breakpoint is instead a start point, then the end point is set to the
838 extreme right side of the sample. The probability density of start points is given
by $f(s_1) = \exp(-Q_0(1 - s_1))/(1 - K(Q_0))$ (Wiuf and Hein 2000, Eq. 6). This
840 function is right-skewed; start points are likely to appear towards the end of the
sampled genome. The CDF and inverse CDF equal:

$$F(S_1) = \frac{1 - \exp(Q_0S_1)}{1 - \exp(Q_0)} \quad (\text{A10})$$

$$F^{-1}(S_1) = \frac{\log(1 + (\exp(Q_0) - 1)S_1)}{Q_0} \quad (\text{A11})$$

842 Before gene conversion is carried through, it is first checked whether it would
result in a sample that does not carry any ancestral material. These fully non-
844 ancestral samples can arise if either (i) conversion acts on an unpaired sample,
in a region spanning entirely non-ancestral material; or (ii) conversion acts over
846 all remaining ancestral material in a paired sample, rendering it non-ancestral.
In case (i) the action stops without creating this ‘ghost’ sample. In case (ii)
848 gene conversion causes a within-individual coalescent event, converting the paired
sample into an unpaired sample. The recipient sample becomes non-ancestral and
850 is no longer tracked.

Deriving probability of ‘complete’ gene conversion

852 Let Q be the mean scaled length of mitotic gene conversion events. Following
Wiuf and Hein (2000), the length of gene conversion events can be drawn from an
854 exponential distribution with parameter Q . Let a gene conversion event start at
a distance x from the focal sequence (where distances are scaled by the number
856 of breakpoints $L - 1$). The gene conversion event will therefore cover the focal
sequence with probability $e^{-Q(1+x)}$. The probability of a complete gene conversion
858 occurring over all paired haplotypes (of which there exist $2(x - k)$), and over the
entire density of conversion breakpoints (of which there exists $g(L - 1)$ per length
860 of focal sequence) equals $2(x - k)g(L - 1) \int_{x=0}^{\infty} e^{-Q(1+x)}$. Solving the integral gives
the probability $2(x - k)(g(L - 1)e^{-Q})/Q$.

862 Note that if $L > 1$ then this probability goes to infinity as $Q \rightarrow 0$. In this case,
the average gene conversion length is much larger than the genetic sample being
864 simulated (i.e., $\lambda \gg L - 1$), so any gene conversion event is likely to affect the
entire genetic region. The reason this discontinuity arises is because the coalescent
866 process assumes that no more than one event occurs per generation. Wiuf and Hein
(2000) ensures this logic is maintained by assuming $Q \sim \mathcal{O}(1)$. Furthermore, a
868 small Q value would invalidate the assumption used to compute Q^* ; specifically,
conversion events that initiate outside the sample but end within it only do so
870 in regions near to the genetic sample (since the probability of these events equals
 e^{-nQ} if initiating $n(L - 1)$ breakpoints away from the sample). Hence while the
872 simulation can be run with very small Q values, it is inadvisable to do so as
erroneous genealogies may be produced.

874 Literature Cited

Abramowitz, M. and I. Stegun, 1970 *Handbook of Mathematical Functions*. Dover
876 Publications, Inc., New York.

Arnaud-Haond, S., C. M. Duarte, F. Alberto, and E. A. Serrão, 2007 Standardizing
878 methods to address clonality in population studies. *Mol. Ecol.* **16**: 5115–5139.

Auton, A. and G. McVean, 2007 Recombination rate estimation in the presence of
880 hotspots. *Genome Res.* **17**: 1219–1227.

Balloux, F., L. Lehmann, and T. de Meeûs, 2003 The population genetics of clonal
882 and partially clonal diploids. *Genetics* **164**: 1635–1644.

Bengtsson, B. O., 2003 Genetic variation in organisms with sexual and asexual
884 reproduction. *J. Evol. Biol.* **16**: 189–199.

Brookfield, J. F. Y., 1992 DNA fingerprinting in clonal organisms. *Mol. Ecol.* **1**:
886 21–26.

Burt, A., D. A. Carter, G. L. Koenig, T. J. White, and J. W. Taylor, 1996 Mo-
888 lecular markers reveal cryptic sex in the human pathogen *Coccidioides immitis*.
Proc. Natl. Acad. Sci. USA **93**: 770–773.

890 Butlin, R., 2002 The costs and benefits of sex: new insights from old asexual
lineages. *Nat. Rev. Genet.* **3**: 311–317.

892 Ceplitis, A., 2003 Coalescence times and the Meselson effect in asexual eukaryotes.
Genet. Res. **82**: 183–190.

- 894 Crease, T. J. and M. Lynch, 1991 Ribosomal DNA variation in *Daphnia pulex*.
Mol. Biol. Evol. **8**: 620–640.
- 896 Duret, L. and N. Galtier, 2009 Biased gene conversion and the evolution of mam-
malian genomic landscapes. Annu. Rev. Genom. Human Genet. **10**: 285–311.
- 898 Flot, J.-F., B. Hespeels, X. Li, B. Noel, I. Arkhipova, *et al.*, 2013 Genomic evidence
for ameiotic evolution in the bdelloid rotifer *Adineta vaga*. Nature **500**: 453–457.
- 900 Frantz, L. A. F., V. E. Mullin, M. Pionnier-Capitan, O. Lebrasseur, M. Ollivier,
et al., 2016 Genomic and archaeological evidence suggest a dual origin of do-
902 mestic dogs. Science **352**: 1228–1231.
- Griffiths, R. C., 1981 Neutral two-locus multiple allele models with recombination.
904 Theor. Popul. Biol. **19**: 169–186.
- Haag, C. R., S. J. McTaggart, A. Didier, T. J. Little, and D. Charlesworth, 2009
906 Nucleotide polymorphism and within-gene recombination in *daphnia magna* and
d. pulex, two cyclical parthenogens. Genetics **182**: 313–323.
- 908 Hartfield, M., 2016 Evolutionary genetic consequences of facultative sex and out-
crossing. J. Evol. Biol. **29**: 5–22.
- 910 Hartfield, M., S. I. Wright, and A. F. Agrawal, 2016 Coalescent times and patterns
of genetic diversity in species with facultative sex: Effects of gene conversion,
912 population structure, and heterogeneity. Genetics **202**: 297–312.
- Hein, J., M. H. Schierup, and C. Wiuf, 2005 *Gene Genealogies, Variation and*
914 *Evolution: A Primer in Coalescent Theory*. Oxford University Press, Oxford.

- Hill, W. G. and A. Robertson, 1968 Linkage disequilibrium in finite populations.
916 Theor. Appl. Genet. **38**: 226–231.
- Hudson, R. R., 1983 Properties of a neutral allele model with intragenic recom-
918 bination. Theor. Popul. Biol. **23**: 183–201.
- Hudson, R. R., 1990 Gene Genealogies and the Coalescent Process. In *Oxford*
920 *Surveys in Evolutionary Biology*, edited by D. J. Futuyma and J. Antonovics,
volume 7, pp. 1–42, Oxford Univ. Press, Oxford.
- 922 Hudson, R. R., 2001 Two-locus sampling distributions and their application. *Ge-*
netics **159**: 1805–1817.
- 924 Hudson, R. R. and N. L. Kaplan, 1985 Statistical properties of the number of
recombination events in the history of a sample of dna sequences. *Genetics* **111**:
926 147–164.
- Jaquiéry, J., S. Stoeckel, C. Rispe, L. Mieuze, F. Legeai, *et al.*, 2012 Accelerated
928 evolution of sex chromosomes in aphids, an X0 system. *Mol. Biol. Evol.* **29**:
837–847.
- 930 Judd, S. R. and T. D. Petes, 1988 Physical lengths of meiotic and mitotic gene
conversion tracts in *Saccharomyces Cerevisiae*. *Genetics* **118**: 401–410.
- 932 Kingman, J. F. C., 1982 On the genealogy of large populations. *J. App. Prob.* **19**:
27–43.
- 934 Lynch, M., R. Gutenkunst, M. Ackerman, K. Spitze, Z. Ye, *et al.*, 2017 Population
genomics of *daphnia pulex*. *Genetics* **206**: 315–332.

936 Mancera, E., R. Bourgon, A. Brozzi, W. Huber, and L. M. Steinmetz, 2008 High-
resolution mapping of meiotic crossovers and non-crossovers in yeast. *Nature*
938 **454**: 479–485.

Mark Welch, D. B. and M. Meselson, 2000 Evidence for the evolution of bdelloid
940 rotifers without sexual reproduction or genetic exchange. *Science* **288**: 1211–
1215.

942 Martini, E., V. Borde, M. Legendre, S. Audic, B. Regnault, *et al.*, 2011 Genome-
Wide Analysis of Heteroduplex DNA in Mismatch Repair-Deficient Yeast Cells
944 Reveals Novel Properties of Meiotic Recombination Pathways. *PLoS Genet.* **7**:
e1002305.

946 McVean, G. A. T., 2002 A genealogical interpretation of linkage disequilibrium.
Genetics **162**: 987–991.

948 McVean, G. A. T., P. Awadalla, and P. Fearnhead, 2002 A coalescent-based method
for detecting and estimating recombination from gene sequences. *Genetics* **160**:
950 1231–1241.

Möhle, M., 1998 A Convergence Theorem for Markov Chains Arising in Population
952 Genetics and the Coalescent with Selfing. *Adv. Appl. Probab.* **30**: 493–512.

Nordborg, M., 1997 Structured coalescent processes on different time scales. *Ge-*
954 *netics* **146**: 1501–1514.

Nordborg, M., 2000 Linkage disequilibrium, gene trees and selfing: An ancestral
956 recombination graph with partial self-fertilization. *Genetics* **154**: 923–929.

- Nordborg, M. and P. Donnelly, 1997 The coalescent process with selfing. *Genetics*
958 **146**: 1185–1195.
- Nordborg, M. and S. M. Krone, 2002 Separation of time scales and convergence to
960 the coalescent in structured populations. *Modern Developments in Theoretical
Population Genetics: The Legacy of Gustave Malécot* pp. 194–232.
- 962 Normark, B. B., 1999 Evolution in a putatively ancient asexual aphid lineage:
Recombination and rapid karyotype change. *Evolution* **53**: 1458–1469.
- 964 Ohta, T. and M. Kimura, 1971 Linkage disequilibrium between two segregating
nucleotide sites under the steady flux of mutations in a finite population. *Ge-*
966 *netics* **68**: 571–580.
- Padhukasahasram, B., P. Marjoram, J. D. Wall, C. D. Bustamante, and M. Nord-
968 borg, 2008 Exploring population genetic models with recombination using effi-
cient forward-time simulations. *Genetics* **178**: 2417–2427.
- 970 Pool, J. E. and C. F. Aquadro, 2006 History and structure of Sub-Saharan popu-
lations of *Drosophila melanogaster*. *Genetics* **174**: 915–929.
- 972 Rosenberg, N. A. and M. Nordborg, 2002 Genealogical trees, coalescent theory
and the analysis of genetic polymorphisms. *Nat. Rev. Genet.* **3**: 380–390.
- 974 Roze, D., 2009 Diploidy, population structure, and the evolution of recombination.
Am. Nat. **174**: S79–S94.
- 976 Roze, D., 2016 Background selection in partially selfing populations. *Genetics* **203**:
937–957.

- 978 Schön, I., R. K. Butlin, H. I. Griffiths, and K. Martens, 1998 Slow molecular
evolution in an ancient asexual ostracod. *Proc. R. Soc. B* **265**: 235–242.
- 980 Schön, I. and K. Martens, 2003 No slave to sex. *Proc. R. Soc. B* **270**: 827–833.
- Simonsen, K. L. and G. A. Churchill, 1997 A markov chain model of coalescence
982 with recombination. *Theor. Popul. Biol.* **52**: 43–59.
- Sunnåker, M., A. G. Busetto, E. Numminen, J. Corander, M. Foll, *et al.*, 2013
984 Approximate Bayesian Computation. *PLoS Comput. Biol.* **9**: e1002803.
- Tsai, I. J., D. Bensasson, A. Burt, and V. Koufopanou, 2008 Population genomics
986 of the wild yeast *Saccharomyces paradoxus*: Quantifying the life cycle. *Proc.*
Natl. Acad. Sci. USA **105**: 4957–4962.
- 988 Tucker, A. E., M. S. Ackerman, B. D. Eads, S. Xu, and M. Lynch, 2013 Population-
genomic insights into the evolutionary origin and fate of obligately asexual *Daph-*
990 *nia pulex*. *Proc. Natl. Acad. Sci. USA* **110**: 15740–15745.
- Veeramah, K. R. and M. F. Hammer, 2014 The impact of whole-genome sequencing
992 on the reconstruction of human population history. *Nat. Rev. Genet.* **15**: 149–
162.
- 994 Wakeley, J., 2009 *Coalescent theory: an introduction*, volume 1. Roberts & Com-
pany Publishers, Greenwood Village, Colorado.
- 996 Wakeley, J. and S. Lessard, 2003 Theory of the effects of population structure and
sampling on patterns of linkage disequilibrium applied to genomic data from
998 humans. *Genetics* **164**: 1043–1053.

Wall, J. D., 2004 Estimating recombination rates using three-site likelihoods. *Ge-*
1000 netics **167**: 1461–1473.

Weir, B. S. and W. G. Hill, 1986 Nonuniform recombination within the human
1002 beta-globin gene cluster. *Am. J. Hum. Gen.* **38**: 776–781.

Wiuf, C. and J. Hein, 2000 The coalescent with gene conversion. *Genetics* **155**:
1004 451–462.